High-pressure helium afterglow at room temperature

R. Deloche, P. Monchicourt, M. Cheret, and F. Lambert
Service de Physique Atomique, Centre d'Etudes Nucléaires de Saclay, 91190 Gif-sur-Yvette, France
(Received 6 August 1975)

The electron-ion recombination mechanisms of He_2^+ are determined along with the rate coefficients of the important elementary processes which govern the relaxation of the helium afterglow, at room temperature. The experimental data (atomic- and molecular-ion currents to the walls, atomic and molecular metastable concentrations, electron concentration, elastic electron collision frequency, electron radiation temperature) obtained as a function of time under a wide range of experimental conditions are compared with the solutions of a system of five coupled partial differential equations which includes all the processes occurring in a helium afterglow. A unique set of rate coefficients and constants is found allowing the precise reproduction of all the experimental data obtained at seven pressures from 5 to 100 Torr. The electron energy balance and electron energy distribution function are calculated as a function of time and space. It is shown that the spatial distribution of the electron energy in our cylindrical experimental cell is not uniform and has to be taken into account, as well as the influence of the non-Maxwellian electrons. The recombination rate coefficient for He_2^+, given under the form $\alpha_2 = (\alpha_{c2} + k_{02} n_0)(T_e/293\ ^\circ\mathrm{K})^{-x_2} + k_{e2} n_e (T_e/293\ ^\circ\mathrm{K})^{-y_2}$, is found to be such that $\alpha_{c2} < 5 \times 10^{-10}$ cm^3/sec, $k_{02} = (5 \pm 1) \times 10^{-27}$ cm^6/sec, $k_{e2} = (4.0 \pm 0.5) \times 10^{-20}$ cm^6/sec, $x_2 = 1 \pm 1$, $y_2 = 4.0 \pm 0.5$. These coefficients correspond to a collisional-radiative model for the recombination of He_2^+ with electrons, which strongly depends on pressure, electron concentration, and electron temperature. 70% of the recombined molecular ions produce atomic metastables corresponding to a dissociation in the lower excited states of the molecule. The rate coefficients for ionizing collisions between metastables are found to be $\beta_{11} = (1.5 \pm 0.3) \times 10^{-9}$ cm^3/sec, $\beta_{22} = (1.5 \pm 0.5) \times 10^{-9}$ cm^3/sec, $\beta_{12} = (2.5 \pm 1.5) \times 10^{-9}$ cm^3/sec. The superelastic electron-metastable rate coefficients are $\gamma_1 = (4.2 \pm 0.6) \times 10^{-9}$ cm^3/sec and $\gamma_2 = (3.8 \pm 0.8) \times 10^{-9}$ cm^3/sec. All the rate coefficients compare very well with available theoretical data. The method used gives a complete solution of the helium afterglow at room temperature. It can be extended in pure helium to many other experimental conditions and applied to the study of afterglows in other pure gases or mixtures.

I. INTRODUCTION

As early as 1949 the development of new techniques of ionization and gas purification together with the introduction of original methods of microwave diagnostics[1] gave a new impulse to the study of glows and afterglows.

Since the measurements by Biondi and Brown[2] a large number of theoretical and experimental works have been devoted to the study of the helium afterglow. Through the years these works have shown a consistent growth of complexity and sophistication of the models necessary to explain the increasing body of experimental data. They were at first directed toward the determination of the ambipolar diffusion coefficient. They immediately encountered and served to reveal the complexity of the mixture of atomic- and molecular-ion concentrations and their variation with time and pressure. Two mechanisms of ion conversion were found experimentally in 1951: one by Phelps and Brown,[3] the other by Hornbeck and Molnar.[4] The ambipolar diffusion coefficients and mobilities of the atomic ion He^+ and of the molecular ion He_2^+ were then measured in various laboratories.[5] The same year a new mechanism of ionization by collision between metastables was proposed by Biondi[6] to explain the production of electrons at the end of a discharge pulse in helium. High concentrations of atomic metastables $He(2\,^1S)$, and $He(2\,^3S)$, and molecular metastables $He_2(2s\,^3\Sigma_u^+)$ contributed to make the interpretation much more complicated in helium afterglows. Conversion and destruction rate coefficients of the metastables have first been measured thoroughly by Phelps[7] under conditions of low electron concentrations. At that time the correlations between ions, metastables, and electron concentrations began to appear.

The electron-ion recombination rate coefficients are generally measured during the relaxation of ionized gases. As early as 1949 Biondi and Brown[2] tried to take into account the electron-ion recombination in the determination of the ambipolar diffusion coefficients. Conversely all the destruction and production processes of charged particles had to be well known to obtain the recombination rate coefficients of the atomic and molecu-

lar ions with electrons.

Gray and Kerr[8] in 1960 gave the first exact interpretation of the decay with time of the average electron density when it is simultaneously controlled by ambipolar diffusion and electron-ion recombination. They showed the importance of the spatial distributions. At this time it had always been assumed that the electron energy distribution function was Maxwellian and that the electron temperature was close to the gas temperature.

Bates and Kingston[9] in 1963 were the first to study the electron energy balance during the afterglow. They showed that the electron temperature is increased by the collisional-radiative electron-stabilized recombination, the theory of which they had published with McWhirter in 1962.[10] Ingraham and Brown[11] later gave the first theoretical model of the electron energy balance in helium afterglows taking into account the predominant heating terms due to the collisional deexcitation of the atomic metastables.

The first attempt to synthesize all the above mechanisms found separately during the helium afterglow is due to Leffel, Hirsh, and Kerr.[12] They first presented a remarkable analysis of the couplings, induced by the previously determined mechanisms, between the concentrations of metastables, electrons, and ions. They indicated the importance of the correlations between these concentrations, the electron energy balance, and the electron energy distribution function.

At low gas pressure (less than 1 Torr) and room temperature, when He^+ is the dominant ion the results of various experiments[12-15] are in rather good agreement. The measurements of the electron-ion recombination rate coefficient are quite well described by the collisional-radiative recombination theory[10] applied to He^+. This model also applies for the atomic ion when it is not the dominant ion, as has been shown at 44.6 Torr by Collins *et al.*[16] Many points, however, remain to be clarified at low pressure, especially the role of the atomic metastables as a source of very energetic electrons, and their influence on the electron energy distribution function and finally on the electron-ion recombination rate coefficient of He^+. The satisfactory agreement between theory and experiment can be probably explained, to a large extent, by the important loss of the non-Maxwellian electrons due to free diffusion.

When the gas pressure is higher than 5 Torr the dominant ion is He_2^+ at room temperature. In analogy to the electron-ion recombination of Ne_2^+ and Ar_2^+, the assumption of a dissociative recombination mechanism for He_2^+ was first proposed. More than four years and a great many experiments[12,14,17-22] have been necessary to demonstrate that the dissociative recombination could not alone explain the previous experimental results on (i) the emitted atomic and molecular spectral light and (ii) the evolution with time of the electron, ion, and metastable concentrations.

Between 5 and 100 Torr the published absolute values of the electron-ion recombination rate coefficient, at room temperature, vary from 10^{-10} to 5.2×10^{-8} cm^3/sec.[2,8,12,18,23-31] Almost all of the mechanisms conceivable have been proposed or invoked to explain these rate coefficients, including (a) the dissociative recombination of He_2^+, (b) the collisional-radiative, electron-stabilized recombination of He_2^+, (c) the collisional-radiative recombination of He_2^+ including neutral-assisted collisional processes, (d) the dissociative recombination of He_3^+, (e) the dissociative recombination of He_2^+ in highly excited vibrational states, the population densities of which would be pressure dependent, and (f) mixtures of these various mechanisms.

The variance between measurements has also been extreme in the observed dependences of the electron-ion recombination rate coefficient. Some experiments have indicated a strong pressure dependence,[25,30] while other studies[31] led to no pressure dependence. Comparable disagreements have been found with regard to the electron density or electron temperature dependences.

The aim of this work has been first to analyze the reasons for this lack of convergence and second to elaborate a method for determination of the unknown mechanisms and rate coefficients corresponding to the degree of the complexity of the helium afterglow due to (i) the strong interactions between the various particle concentrations, (ii) the correlations between these concentrations and the electron energy, and (iii) the couplings between the spatial profiles of the above particle concentrations and the electron energy distribution function.

As a matter of fact it is extremely difficult in such an ionized gas to measure a rate coefficient, to determine a new mechanism, or *a fortiori* to interpret the evolution of the whole afterglow, simply by measuring one or two parameters over a small dynamic range and taking into account only a limited number of physical mechanisms for the interpretation. This is, however, what has been done most frequently and what explains the variance of the results obtained for the recombination of helium molecular ions with electrons. In order to take into account the characteristics of the helium afterglow in the determination of the unknown rate coefficients and especially of the electron-ion recombination of He_2^+, we have first undertaken the measurement as a function of time,

over a wide dynamic range, of all the physical quantities which can presently be reached experimentally, with five different diagnostics. These experimental results have then been interpreted by a system of five coupled partial differential equations. These equations include all the known processes that describe, as functions of time and space, the variation of the concentrations of the atomic and molecular ions, atomic and molecular metastables, and of the electron temperature. The electron energy balance and distribution function have been very carefully studied and calculated as a function of time and space. The non-Maxwellian electrons have been included in the computations.

All the experimental data (more than 40 000 points) obtained at seven different pressures from 5 to 100 Torr and measured at room temperature by microwave interferometry, microwave radiometry, mass spectrometry, and optical absorption and emission spectrometry have been very well reproduced by the proposed system of differential equations, with the same set of rate coefficients and constants. The method we have developed gives a complete solution of the helium afterglow at room temperature, over a wide range of experimental conditions. It shows all the interactions inside the plasma, presents the absolute value and dependences of the electron-ion recombination rate coefficient of He_2^+ and gives the elementary mechanisms responsible for these dependences. It provides the rate coefficients of all the other important elementary processes that describe the helium afterglow relaxation.

In Sec. II we present the mechanisms which have to be taken into account to explain the relaxation of the helium afterglow. In Sec. III we give the energy-transfer mechanisms between electrons, ions, metastables, and ground-state atoms. In Sec. IV we propose a mathematical model, including all the important mechanisms, in order to explain the evolution of the helium afterglow as a function of time and space. In Sec. V we briefly describe the experimental apparatus and measurement techniques. The interpretation of the measurements is given in Sec. VI. In Sec. VII we present the method used to determine the rate constants. The results are shown in Sec. VIII and discussed in Sec. IX.

II. MAIN MECHANISMS IN A HIGH-PRESSURE HELIUM AFTERGLOW

We first describe all the presently known or proposed mechanisms which have to be involved, *a priori*, in our calculations. The comparison between the computed curves and the experimental data will determine among these processes those which must be retained or excluded.

A. Ion conversion

Atomic ions at a concentration n_1 are produced during the discharge pulse, and they are rapidly converted into a concentration of molecular ions, n_2:

$$He^+ + 2He \xrightarrow{\eta} He_2^+(v,K) + He. \quad (1)$$

The frequency rate ηP^2 (P being the pressure) first measured by Phelps and Brown[3] has been extensively studied.[5] The molecular ions are formed in a highly excited vibrational state ($v \sim 15$).

The production of heavy molecular ions is also probably due to the same type of reaction, the rates of which are unknown[32]:

$$He_2^+ + 2He \rightarrow He_3^+ + He, \quad (2)$$

$$He_3^+ + 2He \rightarrow He_4^+ + He. \quad (3)$$

B. Associative ionization

Molecular ions He_2^+ are also formed in collisions between excited atoms and ground-state atoms n_0, as had first been proposed by Hornbeck and Molnar[4]:

$$He^*(p) + He \rightarrow He_2^+(v,K) + e. \quad (4)$$

The corresponding cross sections have been measured for various energy levels p.[33,34] Theoretical and experimental investigations have indicated this process is a nearly resonant reaction, resulting in molecular ions in an excited vibrational state ($v = 4$ for the $3\,^1D$ level). Because of the very small concentrations of the excited atomic species the associative ionization is negligible with respect to the ion conversion (1) in the production of molecular ions.

C. Electron-ion recombination

1. Recombination of atomic ions with electrons

(a) Electron capture and ionization;

$$He^+ + e \rightleftharpoons He^*(p) + h\nu, \quad (5)$$

$$He^+ + e + e \rightleftharpoons He^*(p) + e + KE, \quad (6)$$

$$He^+ + e + He \rightleftharpoons He^*(p) + He + KE. \quad (7)$$

(b) Cascade to the ground state ($p > q$):

$$He^*(p) \rightleftharpoons He^*(q) + h\nu, \quad (8)$$

with a strong reabsorption for transitions to the ground state,

$$He^*(p) + e \rightleftharpoons He^*(q) + e + KE, \quad (9)$$

$$He^*(p) + He \rightleftharpoons He^*(q) + He + KE. \quad (10)$$

Associative ionization has eventually to be taken into account in the electron-ion recombination model of He^+. It will be shown that these collisions are negligible with respect to electronic collisions.

2. Recombination of molecular ions with electrons

The following mechanisms would have to be taken into account simultaneously in an eventual model of the recombination of He_2^+ with electrons.

(a) Electron capture and ionization:

$$He_2^+(v,K)+e \rightleftarrows He_2^*(p,v,K)+h\nu, \quad (11)$$

$$He_2^+(v,K)+e+e \rightleftharpoons He_2^*(p,v,K)+e+KE, \quad (12)$$

$$He_2^+(v,K)+e+He \rightleftharpoons He_2^*(p,v,K)+He+KE. \quad (13)$$

(b) Autoionization:

$$He_2^*(p,v,K) \rightarrow He_2^+(v-1,K)+e+KE. \quad (14)$$

(c) Vibrational relaxation: Collins[34] suggested that sequences of electron capture on a highly excited electronic Rydberg state ($p>10$) followed by autoionization could be a very efficient vibrational relaxation mechanism of the molecular ions, competitive with the vibrational relaxation due to collisions with atoms in the ground state. Stevefelt[35] showed that this mechanism could be fast enough to explain the recently measured associative ionization rates.

$$\begin{aligned} &He_2^+(v,K)+2e \rightarrow He_2^*(p,v,K)+e+KE, \\ &He_2^*(p,v,K) \rightarrow He_2^+(v-1,K)+e+KE. \end{aligned} \quad (15)$$

These two-step sequences of vibrational relaxation provide energy to the free electrons and lead very rapidly to molecular ions in the fundamental vibrational state. Consequently, the excited molecules produced by recombination are in the same $v=0$ state except for the lowest p ($p<8$) and v levels which do not autoionize. The number of possible excited v levels increases when p decreases. This perhaps explains why vibrationally excited molecules have never been observed in a helium afterglow, except for the lowest p levels.

(d) Cascade to the dissociative ground state of the molecule: Several simultaneous stabilization processes can be proposed:

(i) radiative deexcitation ($p>q$),

$$He_2^*(p,v,K) \rightarrow He_2^*(q,v',K')+h\nu; \quad (16)$$

(ii) collisions with electrons ($p>q$),

$$He_2^*(p,v,K)+e \rightleftharpoons He_2^*(q,v,K)+e+KE; \quad (17)$$

(iii) collisions with ground state atoms ($p>q$), giving (iiia) electronic relaxation,

$$He_2^*(p,v,K)+He \rightleftharpoons He_2^*(q,v,K)+He+KE, \quad (18)$$

(iiib) vibrational relaxation,

$$He_2^*(p,v,K)+He \rightleftharpoons He_2^*(p,v-1,K)+He+KE, \quad (19)$$

(iiic) rotational relaxation,

$$He_2^*(p,v,K)+He \rightleftharpoons He_2^*(p,v,K-2)+He+KE \quad (20)$$

($\Delta K=2$ as suggested by Brout[36] and used by Collins[37]).

(e) Dissociation of excited molecules:

$$He_2^*(p,v,K) \rightarrow He^*(p)+He+KE. \quad (21)$$

(f) Dissociative recombination:

$$He_2^+(v,K)+e \rightarrow [He_2^*(p,v,K)] \rightarrow He^*(p)+He+KE, \quad (22)$$

which is the inverse reaction of associative ionization (4).

D. Metastable conversion

Among all the excited atomic and molecular states generated in a helium afterglow, the metastables play an important role because of their high potential energy and high concentrations. Atomic singlet metastables $He(2\,^1S)$ are produced during the discharge pulse in great number densities. However, they are very rapidly converted in collisions with electrons[7]:

$$He(2\,^1S)+e(\mathcal{E}) \rightarrow He(2\,^3S)+e(\mathcal{E}+0.79\ eV). \quad (23)$$

The reaction rate coefficient of this process is so high that the singlet metastables disappear very quickly and become insignificant early in the afterglow, the production term due to recombination being very small compared to this destruction term.

This mechanism may be an important source of energy for the electron gas, in the very early afterglow.

The atomic triplet metastables are also produced by electron-ion recombination. They are converted in molecular metastables M_2 in collisions with two atoms in the ground state[7]:

$$He(2\,^3S)+2He \xrightarrow{\delta} He_2(2s\,^3\Sigma_u)_{v,K}+He. \quad (24)$$

The molecular metastables are probably formed in a highly excited vibrational state.

E. Metastable-metastable ionization

Collisions between helium metastables give an ion and a very energetic electron. Following a proposal of T. Holstein, Biondi[6] first referred to this mechanism to explain the production of elec-

trons in helium after the electric field of the discharge was removed:

$$He(2\,^1S) + He(2\,^1S) \rightarrow He^+ + He + e + 16.6\ eV \quad (25)$$

$$\rightarrow He_2^+(v,K) + e + 19.0\ eV, \quad (26)$$

$$He(2\,^3S) + He(2\,^3S) \rightarrow He^+ + He + e + 15.0\ eV \quad (27)$$

$$\rightarrow He_2^+(v,K) + e + 17.4\ eV, \quad (28)$$

$$He_2(2\,^3\Sigma) + He_2(2\,^3\Sigma) \rightarrow He^+ + 3He + e + 11.3\ eV \quad (29)$$

$$\rightarrow He_2^+(v,K) + 2He + e + 13.7\ eV \quad (30)$$

$$\text{(eventually)} \rightarrow He_3^+ + He + e + 13.8\ eV \quad (31)$$

$$\text{(eventually)} \rightarrow He_4^+ + e + 14.1\ eV. \quad (32)$$

Collisions between different species of metastables have also to be considered:

$$He(2\,^1S) + He(2\,^3S) \rightarrow He^+ + He + e + 15.8\ eV \quad (33)$$

$$\rightarrow He_2^+(v,K) + e + 18.2\ eV, \quad (34)$$

$$He(2\,^1S) + He_2(2\,^3\Sigma) \rightarrow He^+ + 2He + e + 13.9\ eV \quad (35)$$

$$\rightarrow He_2^+(v,K) + He + e + 16.3\ eV \quad (36)$$

$$\text{(eventually)} \rightarrow He_3^+ + e + 16.5\ eV, \quad (37)$$

$$He(2\,^3S) + He_2(2\,^3\Sigma) \rightarrow He^+ + 2He + e + 13.1\ eV \quad (38)$$

$$\rightarrow He_2^+(v,K) + He + e + 15.5\ eV \quad (39)$$

$$\text{(eventually)} \rightarrow He_3^+ + e + 15.7\ eV. \quad (40)$$

The energies of the electrons are given for molecular metastables and molecular ions in the vibrational ground state.

Collisions between atomic triplet metastables have been found to be important and even dominant mechanism in helium afterglows.[3,6,7,15,19,38-45] Johnson and Gerardo[46] emphasized the role played by these collisions and found experimentally a very large rate coefficient, 4.5×10^{-9} cm^3/sec, for the ionizing collisions of two triplet atomic metastables, leading to a total ionizing cross section at 300 °K of about 250 Å^2.

Recent calculations by Garrison *et al.*[47] show that associative ionization (28) at room temperature represents 70% of the total collision rate between two He($2\,^3S$). They also show that the molecular ions are created in a high vibrational ($10 \leq v \leq 19$) and probably high rotational state, which explains why the electron energy distribution is centered around 15.1 instead of 17.4 eV for $v=0$, in this reaction (28). It is interesting to note that the molecular ions He_2^+ are always formed in a highly excited vibrational and rotational state by all the production processes previously mentioned [(1), (4), (26), (28), (30), (34), (36), and (39)]. Garrison *et al.* recently found for the upper limit of the total ionization cross section [(27) and (28)] 94 Å^2, at room temperature, in very good agreement with Phelps's experimental value[38] of 100 Å^2.

F. Collisions between electrons and metastables

1. Excitation to a radiative level

$$\left.\begin{matrix} He(2\,^1S) \\ He(2\,^3S) \end{matrix}\right\} + e + KE \rightarrow He(p) + e$$
$$\Big\downarrow\ p > q$$
$$\text{(ground state)} \leftarrow He(q) + h\nu \quad (41)$$

These reactions do not apply for the atomic metastables, first because the energy gaps between these metastable atoms and the radiative states are very large and require very energetic electrons in sufficient numbers, which is not the case in helium afterglows except under very specific conditions discussed in the next part, and second because the reabsorption of the emitted light due to transitions to the ground state is so strong that nearly all the bound electrons, excited from the atomic metastable state, come back to their initial energy level.

This electronic excitation is more probable for molecular metastables:

$$He_2(2\,^3\Sigma)_{v,K} + e + KE \rightarrow He_2^*(p,v,K) + e$$
$$\Big\downarrow\ p > q$$
$$\text{(ground state)} \leftarrow He_2^*(q,v,K) + h\nu \quad (42)$$

first because the energy required to induce a transition on a radiative level is not as large as in the

atomic case, and second because there is no radiation trapping due to reabsorption, the ground state of the molecule being dissociative.

2. Superelastic deexcitation to the ground state

This mechanism is much more efficient for destroying metastables:

$$He(2\,^1S) + e \rightarrow He + e + 20.6\ eV\,, \tag{43}$$

$$He(2\,^3S) + e \rightarrow He + e + 19.8\ eV\,, \tag{44}$$

$$He_2(2\,^3\Sigma)_{v=0} + e \rightarrow 2He + e + 17.9\ eV\,. \tag{45}$$

Cross sections of process (44) have been deduced[48] from the experimental results of Schultz and Fox[49] and Morrison and Rudge[50] by detailed balancing. The rate coefficients obtained were proportional to the square root of the electron temperature (for $T_e < 2000\ ^\circ K$) and quite small, 6.5×10^{-10} and 1.2×10^{-9} cm^3/sec (Refs. 48 and 51) at room temperature. The classical value of Gryzinsky[52] was 2.2×10^{-9} cm^3/sec, independent of the electron temperature. More recently, Nesbet, Oberoi, and Bardsley[53] deduced the rate coefficient of process (44) from calculations of inelastic electron-atom collision cross sections,[54] which were in excellent agreement with the experimental cross sections obtained by Brongersma *et al.*[55] for the excitation from the helium ground state. They found by detailed balancing that the deactivation rate is nearly constant with temperature and very close to 2.9×10^{-9} cm^3/sec, about 4.5 times the value obtained by Bates *et al.*[48]

G. Collisions between metastables and ground-state helium atoms

As has been shown,[7] collisions with two atoms in the ground state [process (24)] can be an efficient metastable conversion reaction. Destruction of atomic metastables in collisions with only one atom in the ground state seems much more difficult. Such a mechanism would have a much smaller rate coefficient than all the destruction processes previously mentioned. It may be different for the molecular metastables which might undergo collisions described by (18)–(20) or combinations of these three processes.

III. ENERGY OF THE MAIN PARTICLES IN THE AFTERGLOW

The mechanisms we have described induce energy exchanges between charged, excited, and neutral particles as well as conversion between potential and kinetic energy. Consequences of these transfers on the electron and heavy-particle distribution functions have to be determined. Figure 1 shows the scheme of the energy-transfer mechanisms between electrons, ions, and ground-state atoms.

A. Electron energy balance

Many processes, such as collisions between metastables, lead to the production of very energetic, non-Maxwellian electrons. Consequently the electron energy distribution function is not exactly Maxwellian during the afterglow.[56] The departures from a Maxwellian distribution have to be determined as functions of time and space, for each experimental condition, and the energy transfers between thermal and non-Maxwellian electrons have to be calculated.

1. Electron heating mechanisms

(a) Production of non-Maxwellian electrons due to ionization processes: (i) associative ionization (4) and (ii) metastable-metastable ionization (25)–(40).

(b) Production of non-Maxwellian electrons from thermal electrons: (i) electron-ion recombination (6), (9), (12), and (17); (ii) vibrational relaxation of molecular ions (15); (iii) singlet-to-triplet atomic metastable conversion (23); (iv)

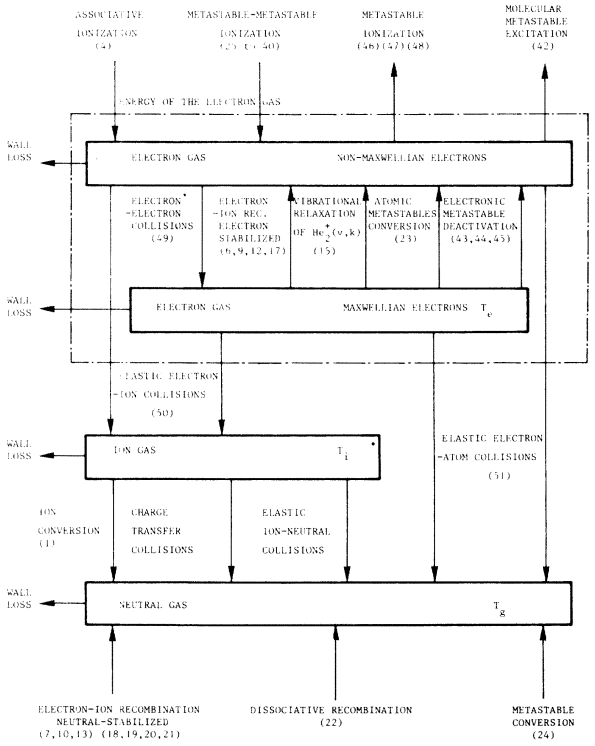

FIG. 1. Scheme of the energy-transfer mechanisms betweem electrons, ions, and ground-state atoms.

superelastic electron metastable collisions (43)–(45).

2. Electron energy-loss mechanisms

(a) Non-Maxwellian electron energy loss:

(i) Electronic excitation of metastables on a radiative level [(41) and (42)].

(ii) Ionization of metastables in collisions with electrons:

$$\mathrm{He}(2\,^1S) + e + (\mathrm{KE} \geq 4.0\ \mathrm{eV}) \rightarrow \mathrm{He}^+ + 2e\,, \quad (46)$$

$$\mathrm{He}(2\,^3S) + e + (\mathrm{KE} \geq 4.8\ \mathrm{eV}) \rightarrow \mathrm{He}^+ + 2e\,, \quad (47)$$

$$\mathrm{He}_2(2\,^3\Sigma) + e + (\mathrm{KE} \geq 4.3\ \mathrm{eV}) \rightarrow \mathrm{He}_2^+ + 2e\,. \quad (48)$$

These last reactions may play a dominant role when the departure from the Maxwellian distribution is large, i.e., when the ratio of metastable to electron concentration is large, as has been observed by Castell and Biondi.[57]

(iii) Electron-electron collisions: These collisions are treated as a continuous energy-loss process between non-Maxwellian and thermal electrons:

$$e(\mathcal{E}_1) + e(\mathcal{E}_2) \rightarrow e(\mathcal{E}_1 - \Delta\mathcal{E}) + e(\mathcal{E}_2 + \Delta\mathcal{E})\,. \quad (49)$$

(iv) Elastic electron-ion collisions,

$$e(\mathcal{E}_1) + \mathrm{ion}(\mathcal{E}_2) \rightarrow e(\mathcal{E}_1 - \Delta\mathcal{E}) + \mathrm{ion}(\mathcal{E}_2 + \Delta\mathcal{E})\,. \quad (50)$$

(v) Elastic electron-atom collisions,

$$e(\mathcal{E}_1) + \mathrm{He}(\mathcal{E}_2) \rightarrow e(\mathcal{E}_1 - \Delta\mathcal{E}) + \mathrm{He}(\mathcal{E}_2 + \Delta\mathcal{E})\,. \quad (51)$$

(vi) Wall losses.

(b) Maxwellian electron energy loss. The Maxwellian electron energy is lost as well in collisions with ions (50) and neutrals (51) along with thermal conductivity. The thermal electrons disappear by diffusion to the walls. The processes (6), (9), (12), (15), (17), (23), and (43)–(45) also lead to a loss of thermal electrons and production of very energetic electrons.

3. Partition of the non-Maxwellian electron energy between the background electrons and neutrals

The energy transferred by a non-Maxwellian electron to the background electron gas and ground-state atoms has been carefully calculated by Wells *et al.*[56] The energy loss of the non-Maxwellian electrons due to the excitation or ionization of metastables [(42) and (46)–(48)] has been neglected in the context of the efficiency of the elastic electron-electron (49) and electron-neutral (51) collisions. This is even more justified when the departure from a Maxwellian distribution is small.

The elastic collisions between "hot" electrons and ions are always negligible. On the other hand the free diffusion of the non-Maxwellian electrons may be an important loss term. Monchicourt, Touzeau, and Wells[58] have shown that, for our experimental conditions, for instance at 10 Torr, 85% of the electrons created at 20 eV and 54% of the electrons produced at 15 eV are lost in free diffusion, for a total electron density of 10^{11} cm^{-3}, assuming a zero-order Bessel function for the spatial distribution. The free diffusion of non-Maxwellian electrons has to be taken into account in the energy partition calculation. It becomes negligible in our experimental conditions above 40 Torr.

4. Electron energy distribution function

The electron energy distribution functions have been calculated both neglecting the diffusion of fast electrons[56] and including it[58] at low pressure. An experimental check of the electron energy distribution function calculated by Monchicourt *et al.*,[58] at 1 Torr, has recently been given by Blagoev *et al.*[59] At a given pressure, the heating of the Maxwellian electrons and the departure from a Maxwellian distribution function depend on the metastable to electron concentration ratio and on the efficiency of the diffusion of fast electrons.

5. Energy balance of the Maxwellian electrons

The electron temperature can be calculated as a function of time and space if one knows (a) the production rate coefficients of the non-Maxwellian electrons, (b) the energy they transfer to the thermal electrons, (c) the ion and atom temperatures, (d) the total electron concentration, (e) the concentrations of ions, metastables, and atoms in the ground state, and (f) the spatial distributions of these parameters.

The couplings between the particle concentrations and the correlations between these concentrations and the potential or kinetic energy of the various particles are emphasized in the determination of the Maxwellian electron energy balance. Because of the spatial profiles of the particle concentrations, the electron energy distribution functions and electron temperatures vary with time and space. The production of non-Maxwellian electrons during the afterglow slows down the electron temperature decay.

B. Energy balance of the ground-state atoms

As shown in Fig. 1, atoms in the ground state can be heated by many different mechanisms, but it has not been necessary to determine precisely the amounts of energy exchanged in each reaction,

the atom concentrations being large (10^{17}–10^{18} cm^{-3}) and the wall loss quite important. Only the energy provided during the discharge pulse would be able to slightly increase the gas temperature. We have checked experimentally that the gas temperature T_g is always very close to the ambiant temperature T_a. The gas temperature in this work is uniform and equal to 293 ± 1 °K.

C. Energy balance of the ions

The ions are heated by electron-ion elastic collisions and are cooled by very efficient processes, (i) elastic collisions with ground-state atoms and (ii) wall loss. The ion temperature T_i is always equal to the gas temperature, $T_i = T_g = T_a = 293$ °K.

IV. SYSTEM OF COUPLED DIFFERENTIAL EQUATIONS

In order to describe the evolution with time of the main parameters simultaneously during the helium afterglow, it is necessary to include in the theoretical model all the processes presented in Secs. II and III with the corresponding couplings and the geometrical characteristics of the ionized gas. We are then concerned with a system of coupled partial differential equations. To limit the number of equations and to simplify as much as possible this system, we have assumed that (i) the geometry of the ionized gas under study is an infinite cylinder; (ii) the plasma is perfectly centered, the spatial profiles having a cylindrical symmetry; (iii) there are no ions other than He^+ and $He_2^+(v,K)$ at room temperature, and the traces of heavy molecular helium are neglected along with impurities; the helium gas is considered as perfectly pure; (iv) the charge density equals zero in each elementary volume of the ionized gas, $n_e = n_1 + n_2$; (v) ions and ground-state atoms have the same uniform temperature equal to the ambiant temperature, $T_i = T_g = T_a = 293$ °K; and (vi) on the walls, the charged- or excited-particle concentrations are null and the electron temperature tends to the gas temperature. As we shall see, these assumptions are compatible with our experimental conditions.

The helium afterglow can then be described by the simultaneous study with time t and space r of: (A) the electron concentration $n_e(r,t)$, (B) the atomic-ion concentration $n_1(r,t)$, (C) the molecular-ion concentration $n_2(r,t)$, (D) the atomic-metastable concentration $M_1(r,t)$, (E) the molecular-metastable concentration $M_2(r,t)$, and (F) the electron temperature $T_e(r,t)$.

Since we always assume $n_e(r,t) = n_1(r,t) + n_2(r,t)$, we have to solve a system of five coupled partial differential equations.

A. Continuity equation for the atomic-ion He^+ density $n_1(r,t)$

The relaxation of atomic ions is due to (Fig. 2) the following sources:

(a) Diffusion,

$$\left(\frac{\partial n_1(r,t)}{\partial t}\right)_{\text{dif}} = D_1 \nabla \left[\left(1 + \frac{T_e(r,t)}{T_g}\right) \nabla n_1(r,t) \right],$$

with D_1 the diffusion coefficient in cm^2/sec.

(b) Electron-ion recombination [processes (4)–(10)],

$$\left(\frac{\partial n_1(r,t)}{\partial t}\right)_{\text{rec}} = -\alpha_1 n_e(r,t) n_1(r,t),$$

where for the electron-ion recombination rate coefficient α_1 we have used the formula obtained by Collins *et al.*,[16]

$$\alpha_1 = 8.1 \times 10^{-20} \frac{n_e(r,t)}{1 + 0.079P} \left(\frac{T_e(r,t)}{T_g}\right)^{-4.4},$$

with α_1 in cm^3/sec, $n_e(r,t)$ in cm^{-3}, and P in Torr. The recombination rate coefficient α_1 can also be written, in the first approximation, for our experimental conditions, in the most general form

$$\alpha_1 = \alpha_{01} \left(\frac{T_e(r,t)}{T_g}\right)^{-x_1} + k_{e1} \left(\frac{T_e(r,t)}{T_g}\right)^{-y_1} n_e(r,t),$$

with $\alpha_{01} = \alpha_{c1} + k_{01} n_0$. α_{c1} (cm^3/sec) is a constant

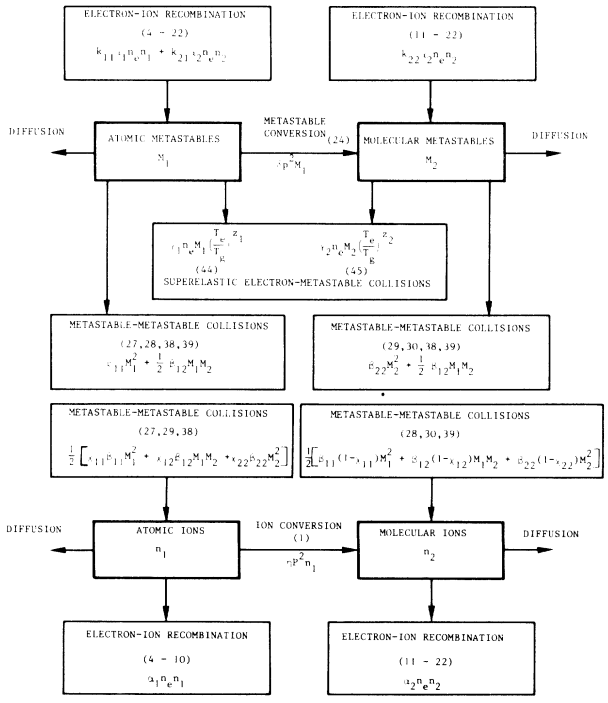

FIG. 2. Scheme of the couplings between helium metastables and ions.

recombination rate coefficient mainly due to the radiative mechanisms; k_{01} (cm^6/sec) is the neutral-assisted recombination rate coefficient (n_0 in cm^{-3} is the ground-state-atom concentration); and k_{e1} (cm^6/sec) is the electron-assisted recombination rate coefficient.

As a matter of fact, Deloche[60] has shown that the recombination rate coefficient, for our experimental conditions, could be written as the sum of these three terms, for $T_e = T_g$ and in the case of a simple model of the helium molecule. Collins[61] reached the same conclusions in the calculation of α_1, assuming the electron temperature is varied from 2000 °K to gas temperature, 300 °K. In the case of the atomic ion He^+, α_{c1} and k_{01} are probably very small with regard to k_{e1}, as can be deduced from the previous measurements at low pressure. We have assumed α_{c1} and k_{01} have the same electron temperature dependence x_1, which is not rigorous, but represents the expected limit of sensitivity of our method.

(c) Ion conversion (1),

$$\left(\frac{\partial n_1(r,t)}{\partial t}\right)_{\text{conv}} = -\eta P^2 n_1(r,t).$$

During the afterglow, atomic ions are produced in collisions between metastables [(25), (27), (29), (33), (35), and (38)]. For our experimental conditions, the atomic singlet metastables $He(2\,^1S)$ are very rapidly converted into triplet metastables ($2\,^3S$). They disappear so quickly that they become insignificant early in the afterglow. They are always negligible even at 5 Torr. χ_{11}, χ_{12}, and χ_{22} are the respective percentages of creation of atomic ions in the processes (27), (38), and (29):

$$\left(\frac{\partial n_1(r,t)}{\partial t}\right)_{MM} = +\tfrac{1}{2}[\chi_{11}\beta_{11}M_1^2(r,t) + \chi_{12}\beta_{12}M_1(r,t)M_2(r,t) + \chi_{22}\beta_{22}M_2^2(r,t)].$$

M_1 is the atomic-triplet-metastable concentration $He(2\,^3S)$ only; M_2 represents the molecular-metastable concentration.

B. Continuity equation for the molecular-ion He_2^+ density $n_2(r,t)$

During the afterglow the molecular ions He_2^+ are destroyed by (a) diffusion (Fig. 2),

$$\left(\frac{\partial n_2(r,t)}{\partial t}\right)_{\text{dif}} = D_2\nabla\left[\left(1+\frac{T_e(r,t)}{T_g}\right)\nabla n_2(r,t)\right],$$

with D_2 being the diffusion coefficient in cm^2/sec; (b) electron-ion recombination [(11)–(22)],

$$\left(\frac{\partial n_2(r,t)}{\partial t}\right)_{\text{rec}} = \alpha_2 n_e(r,t) n_2(r,t).$$

Molecular ions are always formed in highly excited vibrational and rotational states [(1), (4), (26), (28), (30), (34), (36), and (39)]. Many mechanisms [(11)–(22)] may be important in the electron capture and stabilization of the recombination. In order not to prejudge the relative importance of these various processes, the recombination rate coefficient α_2 has been written in the general form

$$\alpha_2 = \alpha_{02}\left(\frac{T_e(r,t)}{T_g}\right)^{-x_2} + k_{e2}n_e(r,t)\left(\frac{T_e(r,t)}{T_g}\right)^{-y_2},$$

with $\alpha_{02} = \alpha_{c2} + k_{02}n_0$. α_{c2} is independent of n_0 or n_e; it represents, for instance, the radiative [(11) and (16)] and dissociative [(21) and (22)] parts of the recombination. k_{02} corresponds to the neutral-assisted part of the recombination [(13) and (18)–(20)]. k_{e2} is the electron-assisted part of the recombination rate coefficient α_2 [(12) and (17)].

The unique *a priori* assumptions were first that α_2 could be written under the sum of three terms, which seems justified for our experimental conditions,[60,61] and second that α_{c2} and k_{02} had the same electron temperature dependence x_2. The determination of a small difference in the electron temperature dependence of these two coefficients seemed beyond the sensitivity of the proposed method.

The molecular ions are produced in the following reactions (Fig. 2) (a) atomic-ion conversion (1),

$$\left(\frac{\partial n_2(r,t)}{\partial t}\right)_{\text{conv}} = +\eta P^2 n_1(r,t);$$

(b) collisions between metastables [(28), (30), and (39)] neglecting the formation of heavy molecular ions [(31), (32), and (40)],

$$\left(\frac{\partial n_2(r,t)}{\partial t}\right)_{MM} = +\tfrac{1}{2}[(1-\chi_{11})\beta_{11}M_1^2(r,t) + (1-\chi_{12})\beta_{12}M_1(r,t)M_2(r,t) + (1-\chi_{22})\beta_{22}M_2^2(r,t)].$$

C. Continuity equation for the atomic-metastable concentration

The atomic-triplet-metastable $M_1(r,t)$ relaxation is due to (Fig. 2) (a) diffusion,

$$\left(\frac{\partial M_1(r,t)}{\partial t}\right)_{\text{dif}} = D_{M_1}\nabla^2 M_1(r,t);$$

(b) collisions between atomic metastables [(27) and (28)],

$$\left(\frac{\partial M_1(r,t)}{\partial t}\right)_{M_1-M_1} = -\beta_{11}M_1^2(r,t);$$

(c) collisions with a molecular metastable [(38), and (39)],

$$\left(\frac{\partial M_1(r,t)}{\partial t}\right)_{M_1-M_2} = -\tfrac{1}{2}\beta_{12}M_1(r,t)M_2(r,t),$$

where the reaction (40) is neglected; (d) superelastic electron-metastable collision (44),

$$\left(\frac{\partial M_1(r,t)}{\partial t}\right)_{e-M_1} = -\gamma_1 M_1(r,t)n_e(r,t)\left(\frac{T_e(r,t)}{T_g}\right)^{z_1},$$

with $0 \leq z_1 \leq 0.5$; and (e) conversion into molecular metastable (24),

$$\left(\frac{\partial M_1(r,t)}{\partial t}\right)_{\text{conv}} = -\delta P^2 M_1(r,t).$$

The atomic metastables are produced by the following mechanisms (Fig. 2): (a) recombination of atomic ions with electrons [(4)–(10)],

$$\left(\frac{\partial M_1(r,t)}{\partial t}\right)_{\text{rec}} = +k_{11}\alpha_1 n_e(r,t)n_1(r,t),$$

where k_{11} is the proportion of the recombined atomic ions giving atomic metastables; and (b) recombination of molecular ions [(11)–(22)] including the dissociation of an excited helium molecule (21) or the dissociative recombination (22),

$$\left(\frac{\partial M_1(r,t)}{\partial t}\right)_{\text{rec}} = +k_{21}\alpha_2 n_e(r,t)n_2(r,t),$$

where k_{21} represents the proportion of molecular ions n_2 which give atomic metastables by recombination.

D. Continuity equation for the molecular-metastable density

The molecular-metastable concentration $M_2(r,t)$ decreases by (Fig. 2) (a) diffusion,

$$\left(\frac{\partial M_2(r,t)}{\partial t}\right)_{\text{dif}} = D_{M_2}\nabla^2 M_2(r,t);$$

(b) collisions between molecular metastables [(29) and (30)],

$$\left(\frac{\partial M_2(r,t)}{\partial t}\right)_{M_2-M_2} = -\beta_{22}M_2^2(r,t),$$

where the reactions [(31) and (32)] leading to heavy molecular ions are neglected; (c) collisions with an atomic metastable [(38) and (39)],

$$\left(\frac{\partial M_2(r,t)}{\partial t}\right)_{M_1-M_2} = -\tfrac{1}{2}\beta_{12}M_1(r,t)M_2(r,t);$$

and (d) superelastic electron-metastable collision (45),

$$\left(\frac{\partial M_2(r,t)}{\partial t}\right)_{e-M_2} = -\gamma_2 M_2(r,t)\, n_e(r,t)\left(\frac{T_e(r,t)}{T_g}\right)^{z_2}$$

where a slight contribution to γ_2 could be provided by reactions [(42) and (48)] if the departure from a Maxwellian distribution became important.

The molecular metastables are produced by (Fig. 2) (a) atomic-metastable conversion (24),

$$\left(\frac{\partial M_2(r,t)}{\partial t}\right)_{\text{conv}} = +\delta P^2 M_1(r,t);$$

(b) electron-ion He_2^+ recombination [(11)–(22)],

$$\left(\frac{\partial M_2(r,t)}{\partial t}\right)_{\text{rec}} = +k_{22}\alpha_2 n_e(r,t)n_2(r,t),$$

where k_{22} is the proportion of the recombined molecular ions which give molecular metastables. The sum $k_{21}+k_{22}$ may be slightly less than 1 because of the radiative transitions to the ground state, in the singlet molecular system.

E. Continuity equation for the electron temperature $T_e(r,t)$

See Fig. 3 and Ref. 57. The total energy of the Maxwellian electrons included, at time t, in an elementary volume dV located at a distance r from the axis of the cell is

$$U_e(r,t) = \tfrac{3}{2}kT_e(r,t)n_e(r,t).$$

Its variation with time is

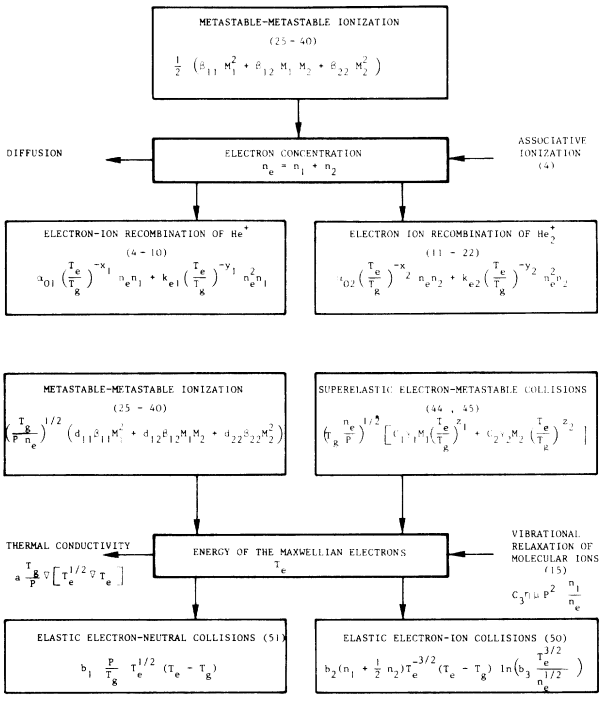

FIG. 3. Scheme of the production and destruction terms of the electron concentration, along with the heating and cooling terms of the Maxwellian electrons.

$$\frac{\partial U_e(r,t)}{\partial t} = \tfrac{3}{2}kT_e(r,t)\frac{\partial n_e(r,t)}{\partial t} + \tfrac{3}{2}kn_e(r,t)\frac{\partial T_e(r,t)}{\partial t}.$$

The first term of this sum represents the loss of the Maxwellian electrons, calculated in the continuity equations for the atomic and molecular ions ($n_e = n_1 + n_2$). The variation with time of the electron temperature, included in the second term of the sum, is now determined.

The electron temperature decay is due to (Fig. 3) the following sources:

(a) Thermal conductivity,

$$\left(\frac{\partial T_e(r,t)}{\partial t}\right)_{TC} = \nabla[D_e(r,t)\nabla T_e(r,t)],$$

with

$$D_e(r,t) = \tfrac{2}{3}\times 3.37\frac{kT_e(r,t)}{m\langle\nu_{e0}(r,t)\rangle}$$

(see Refs. 62 and 63), and

$$\langle\nu_{e0}(r,t)\rangle = \tfrac{4}{3}n_0\sigma_{e0}\left(\frac{8kT_e(r,t)}{\pi m}\right)^{1/2},$$

with $\sigma_{e0} = 5.6\times10^{-16}$ cm^2. The electron-ion collision frequency can be neglected here even at 5.0 Torr:

$$\left(\frac{\partial T_e(r,t)}{\partial t}\right)_{TC} = a(T_g/P)\nabla[T_e(r,t)^{1/2}\nabla T_e(r,t)],$$

with $a = 75.61$ cgs.

(b) Elastic electron-neutral collisions (51),

$$\left(\frac{\partial T_e(r,t)}{\partial t}\right)_{e0} = -2(m/M)\langle\nu_{e0}(r,t)\rangle[T_e(r,t) - T_g]$$
$$= -b_1(P/T_g)[T_e(r,t)]^{1/2}[T_e(r,t) - T_g],$$

with $b_1 = 1.22\times10^6$ cgs.

(c) Elastic electron-ion collisions (50),

$$\left(\frac{\partial T_e(r,t)}{\partial t}\right)_{ei} = -\frac{2m}{M}\langle\nu_{ei}(r,t)\rangle[T_e(r,t) - T_g]$$
$$= -b_2[n_1(r,t) + \tfrac{1}{2}n_2(r,t)]T_e^{-3/2}(r,t)$$
$$\times[T_e(r,t) - T_g]\ln\left[b_3\frac{T_e^{3/2}(r,t)}{n_e^{1/2}(r,t)}\right],$$

with $b_2 = 9.89\times10^{-4}$ cgs and $b_3 = 8.26\times10^3$ cgs (see the Appendix).

A small part of the energy of the non-Maxwellian electrons is transferred to the thermal electrons through the electron-electron collisions (49). This energy transfer $\Delta\mathcal{E}(r,t)$ depends somewhat on the initial energy of the very energetic electrons produced during the afterglow.

In first approximation, if the free diffusion of these non-Maxwellian electrons is neglected, the energy transferred to the background electron gas can be taken as (Fig. 4)

$$\Delta\mathcal{E}(r,t) = 1.385\times10^{-6}[n_e(r,t)T_g/P]^{1/2}, \qquad (52)$$

independent of the initial energy of the non-Maxwellian electrons created between 15 an 20 eV, when $n_e(r,t)/P \leq 2\times10^{11}$ cm^{-3} Torr^{-1}, which is always verified in our experimental conditions. This formula (52) slightly overestimates the energy transferred to the thermal electrons when the initial energy of the non-Maxwellian electrons is less than 15 eV, as shown in Fig. 4.

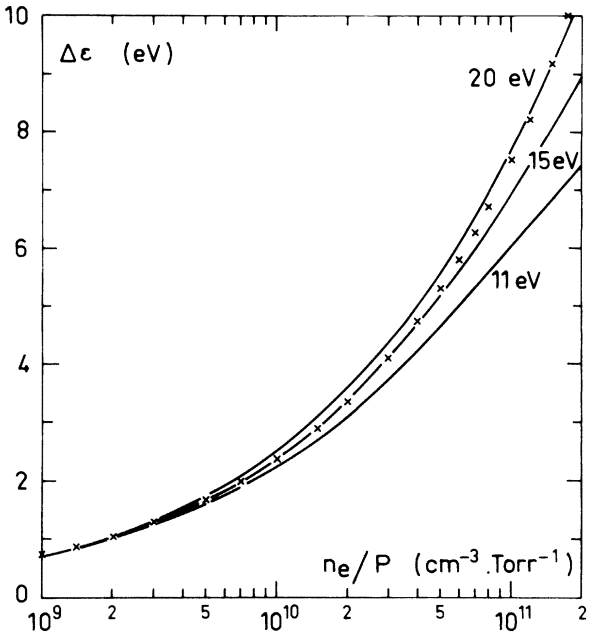

FIG. 4. Energy transferred $\Delta\mathcal{E}$ to the Maxwellian electrons (at 300°K) by the relaxation of non-Maxwellian electrons when the free diffusion is negligible, as a function of the ratio n_e/P (cm^{-3} Torr^{-1}), for different values of the initial energy of the "hot" electrons. Full lines represent exact calculations. Crosses (×) give the energy transfer as calculated by formula (52) independent of the initial electron energy.

(a) Heating of the Maxwellian electrons due to collisions between electrons and atomic metastables (44) (Fig. 3):

$$\tfrac{3}{2}kn_e(r,t)\left(\frac{\partial T_e(r,t)}{\partial t}\right)_{e-M_1} = +\gamma_1 M_1(r,t)n_e(r,t)\left(\frac{T_e(r,t)}{T_g}\right)^{z_1}\Delta\mathcal{E}(r,t).$$

In this case the energy transferred to the background electron gas is very well approximated by the relation (52),

$$\left(\frac{\partial T_e(r,t)}{\partial t}\right)_{e-M_1} = +C_1\gamma_1\left(\frac{T_g}{P}\right)^{1/2} M_1(r,t)n_e(r,t)^{1/2}\left(\frac{T_e(r,t)}{T_g}\right)^{z_1},$$

with $C_1 = 1.07\times10^{-2}$ cgs.

(b) Heating of the Maxwellian electrons due to superelastic collisions between electrons and molecular metastables (45) (Fig. 3). In this case formula (52) also applies very well,

$$\left(\frac{\partial T_e(r,t)}{\partial t}\right)_{e-M_2} = +C_2\gamma_2\left(\frac{T_g}{P}\right)^{1/2} M_2(r,t)n_e(r,t)^{1/2}\left(\frac{T_e(r,t)}{T_g}\right)^{z_2},$$

with $C_2 = C_1$.

(c) Heating of the Maxwellian electrons due to metastable-metastable ionization [(27)–(30), (38), and (39)] (Fig. 3):

$$\begin{aligned}\tfrac{3}{2}kn_e(r,t)\left(\frac{\partial T_e(r,t)}{\partial t}\right)_{MM} = \tfrac{1}{2}[&\chi_{11}\beta_{11}M_1^2(r,t)\Delta\mathcal{E}_{111}(r,t) + (1-\chi_{11})\beta_{11}M_1^2(r,t)\Delta\mathcal{E}_{112}(r,t)\\ &+\chi_{12}\beta_{12}M_1(r,t)M_2(r,t)\Delta\mathcal{E}_{121}(r,t) + (1-\chi_{12})\beta_{12}M_1(r,t)M_2(r,t)\Delta\mathcal{E}_{122}(r,t)\\ &+\chi_{22}\beta_{22}M_2^2(r,t)\Delta\mathcal{E}_{221}(r,t) + (1-\chi_{22})\beta_{22}M_2^2(r,t)\Delta\mathcal{E}_{222}(r,t)].\end{aligned}$$

The six values of $\Delta\mathcal{E}(r,t)$ correspond, respectively, to the processes (27) and (28), (38) and (39), (29) and (30). They represent the amount of energy transferred from non-Maxwellian electrons produced with initial energies between 11.3 and 17.4 eV. However, the most probable initial energy of the electrons created in these six processes is close to 15 eV: It has been shown[47] in the case of atomic metastables [(27) and (28)] that the molecular ion He_2^+ is probably produced in a high vibrational and rotational state. For the collisions between two molecular metastables the process (30) is more probable than (29) and the molecular metastables are also produced in highly excited vibrational and rotational states, thus increasing the energy of the ejected electron. This also applies for reactions (38) and (39). In first approximation we may then assume the energy transfer is the same for these six reactions and use the formula (52). In the worst case, the overestimation of the energy transfer is then about 15%, at low pressure, high electron density, and for collisions between molecular metastables. An exact calculation of the energy transfer could be done, knowing precisely the initial energy of the electron released in each reaction:

$$\begin{aligned}\left(\frac{\partial T_e(r,t)}{\partial t}\right)_{MM} = &\left(\frac{T_g}{P}\right)^{1/2} n_e(r,t)^{-1/2}\\ &\times[d_{11}\beta_{11}M_1^2(r,t) + d_{12}\beta_{12}M_1(r,t)M_2(r,t)\\ &+ d_{22}\beta_{22}M_2^2(r,t)]\end{aligned}$$

with $d_{11} = d_{12} = d_{22} = 5.36\times10^{-3}$ cgs.

(d) Heating of the Maxwellian electrons due to vibrational relaxation of the molecular ions (15): Each process of mechanism (15) provides a small amount of energy to the electron released. These small quantities of energy are entirely transferred to the Maxwellian electrons. Under these conditions, each molecular ion provides 2.387 eV at the maximum, when produced in the highest vibrational excited state, as is probably the case for reaction (1):

$$\tfrac{3}{2}kn_e(r,t)\left(\frac{\partial T_e(r,t)}{\partial t}\right)_{VR} = +\,2.387\eta P^2 n_1(r,t)\mu,$$

$$0 \leq \mu \leq 1$$

$$\left(\frac{\partial T_e(r,t)}{\partial t}\right)_{VR} = C_3\mu\eta P^2\frac{n_1(r,t)}{n_e(r,t)},$$

with $C_3 = 1.85\times10^4$ cgs.

In this form, the heating term due to the vibrational relaxation of the molecular ions is probably underestimated if mechanism (15) is effectively competitive with ground-state-atom collisions. As a matter of fact, molecular ions are always created in highly excited vibrational and rotational states, for instance in collisions between metastables. In these reactions [(28), (30), and (39)],

$$M + M \rightarrow He_2^+(v,K) + e + \mathrm{KE},$$

the energy transferred to the background electron gas from the very energetic emitted electron does not change much with the initial energy of this electron, but the energy transfer due to the vibrational relaxation of the molecular ion directly depends on the initial vibrational state v. This vibrational energy is entirely given to the thermal electrons if mechanism (15) really applies. The vibrational relaxation of the molecular ions and excited molecules in autoionizing levels increases the electron temperature but does not modify the tail of the electron energy distribution function.

At low gas pressure the loss of "hot electrons" due to free diffusion has to be taken into account.[58] The electron energy $\Delta\mathcal{E}(r,t)$ transferred to the

Maxwellian electrons decreases and formula (52) is no longer valid. At 5 Torr the energy transfer has been approximated by

$$\Delta\mathcal{E}(r,t) = 3.33\times10^{-14} n_e(r,t) T_g/P$$

for initial electron energy from 18 to 20 eV, and

$$\Delta\mathcal{E}(r,t) = 5.67\times10^{-14} n_e(r,t) T_g/P$$

for initial electron energy equal to or less than 15 eV. At 10, 20, and 40 Torr a good approximation consists in dividing the formula (52) by a constant factor: 2.0 for electrons created between 18 and 20 eV, at 10 Torr, 1.8 for electrons created at 15 eV or less, at 10 Torr, 1.2 at 20 Torr, independent of the initial electron energy, and 1.05 at 40 Torr, independent of the initial electron energy.

The system of coupled partial differential equations we propose to describe the characteristics of the helium afterglow at room temperature and pressures from 5 to 100 Torr is the following:

$$n_e = n_1 + n_2 ,$$

$$\frac{dn_1}{dt} = D_1\nabla\left[\left(1+\frac{T_e}{T_g}\right)\nabla n_1\right] - \alpha_{01}\left(\frac{T_e}{T_g}\right)^{-x_1} n_e n_1 - k_{e1}\left(\frac{T_e}{T_g}\right)^{-y_1} n_e^2 n_1 - \eta P^2 n_1 + \tfrac{1}{2}(\chi_{11}\beta_{11}M_1^2 + \chi_{12}\beta_{12}M_1M_2 + \chi_{22}\beta_{22}M_2^2) ,$$

$$\frac{dn_2}{dt} = D_2\nabla\left[\left(1+\frac{T_e}{T_g}\right)\nabla n_2\right] - \alpha_{02}\left(\frac{T_e}{T_g}\right)^{-x_2} n_e n_2 - k_{e2}\left(\frac{T_e}{T_g}\right)^{-y_2} n_e^2 n_2 + \eta P^2 n_1$$
$$+ \tfrac{1}{2}[(1-\chi_{11})\beta_{11}M_1^2 + (1-\chi_{12})\beta_{12}M_1M_2 + (1-\chi_{22})\beta_{22}M_2^2] ,$$

$$\frac{dM_1}{dt} = D_{M_1}\nabla^2 M_1 - \beta_{11}M_1^2 - \tfrac{1}{2}\beta_{12}M_1M_2 - \gamma_1\left(\frac{T_e}{T_g}\right)^{+z_1} n_e M_1 - \delta P^2 M_1 + k_{11}\alpha_1 n_e n_1 + k_{21}\alpha_2 n_e n_2 ,$$

$$\frac{dM_2}{dt} = D_{M_2}\nabla^2 M_2 - \beta_{22}M_2^2 - \tfrac{1}{2}\beta_{12}M_1M_2 - \gamma_2\left(\frac{T_e}{T_g}\right)^{+z_2} n_e M_2 + \delta P^2 M_1 + k_{22}\alpha_2 n_e n_2 ,$$

$$\frac{dT_e}{dt} = a\frac{T_g}{P}\nabla(T_e^{1/2}\nabla T_e) - b_1\frac{P}{T_g}T_e^{1/2}(T_e - T_g) - b_2(n_1 + \tfrac{1}{2}n_2)T_e^{-3/2}(T_e - T_g)\ln\left(b_3\frac{T_e^{3/2}}{n_e^{1/2}}\right) + c_1\left(\frac{T_g}{P}\right)^{1/2}\gamma_1 n_e^{1/2} M_1\left(\frac{T_e}{T_g}\right)^{+z_1}$$
$$+ c_2\left(\frac{T_g}{P}\right)^{1/2}\gamma_2 n_e^{1/2} M_2\left(\frac{T_e}{T_g}\right)^{+z_2} + c_3\mu\eta P^2\frac{n_1}{n_e} + d_{11}\left(\frac{T_g}{P}\right)^{1/2}\beta_{11}n_e^{-1/2}M_1^2$$
$$+ d_{12}\left(\frac{T_g}{P}\right)^{1/2}\beta_{12}n_e^{-1/2}M_1M_2 + d_{22}\left(\frac{T_g}{P}\right)^{1/2}\beta_{22}n_e^{-1/2}M_2^2 ,$$

where n_1, n_2, n_e, M_1, M_2, and T_e are functions of time and space.

If the above analysis is right this system of differential equations should allow the reproduction *with the same set of rate coefficients and constants* of all the experimental data measured as a function of time with the five different diagnostics. The comparison between calculations and experiment should also allow the exclusion of the processes taken into account which do not occur during the helium afterglow or, on the contrary, show that an important process is missing or has been improperly neglected.

V. EXPERIMENTAL APPARATUS AND MEASUREMENT TECHNIQUES

From the above analysis of the helium afterglow the main parameters to be measured are the ground-state-atom concentration n_0 (cm^{-3}) given by the pressure P (Torr) and the gas temperature T_g (°K), the atomic n_1 and molecular n_2 ion concentrations (cm^{-3}), eventually the heavy-molecular-ion concentrations, the atomic M_1 and molecular M_2 metastable number densities (cm^{-3}), the electron density n_e (cm^{-3}), and the electron temperature T_e (°K). The excited-state population densities of atoms and molecules are also necessary to give an accurate interpretation of the electron-ion recombination rate coefficients.

Two experimental apparatus have been used. One of them has been previously described[24,25] and a brief summary of their common characteristics is given here for convenience. After baking (400 °C), the ultimate residual pressure in the two identical experimental chambers is better than 10^{-9} Torr. Helium is successively purified in two water-cooled cataphoresis tubes before it is introduced in the cylindrical experimental cells (1.832-cm i.d., 30.00 cm between electrode passages, 40 cm long). The impurity concentration is then less than 10^{-8} of the helium-atom concentration. The gas is ionized by high-voltage dc pulses. The time duration, the repetition rate, and the voltage amplitude of the pulses are adjustable[64] to obtain the best discharge conditions for each pressure.

Capacitance manometers and a fused-quartz Bourdon pressure gauge have been used to measure the pressure. The precision is always better than 0.1 Torr. The high degree of accuracy of the fused-quartz Bourdon capsule allowed us to check that the increase of the average gas temperature in the experimental chambers is always less than 1 °K. One of the two experimental apparatus was devoted to the microwave diagnostics, the other one to the mass-spectrometry measurements. The same optical absorption and emission spectrometry techniques have been developed on both experiments. They have been used, at each investigated pressure, to verify the identity of the experimental conditions during the afterglow in the two experimental cells. The measurement techniques which have been performed are now briefly described.

A. *X*-band microwave interferometry

The axis of the cylindrical quartz experimental chamber is very well centered in an oversized waveguide (3.00×3.00 cm^2). *X*-band microwave interferometry has been used to measure the decay with time of (i) the average attenuation $\langle A(t)\rangle$ in dB and (ii) the average phase shift $\langle\varphi(t)\rangle$ in degrees for the wave crossing the plasma branch.

At a given time, these two quantities only depend on the spatial distribution of the electron concentration and electron energy, on the microwave propagating mode, and on the electron energy distribution function. We have applied the well-known theory of electromagnetic wave propagation in plasmas,[65] but we have taken into account the spatial distribution of the electron energy and calculated the influence of the non-Maxwellian electrons on the value of the average physical quantities directly comparable to the experiment. The average elastic electron-ion and electron-neutral collision frequency $\langle\nu(t)\rangle$ and the average "effective" electron concentration $\langle n_e^{\text{eff}}(t)\rangle$ are directly deduced from the measurements of $\langle A(t)\rangle$ and $\langle\varphi(t)\rangle$ without any assumption other than small perturbations of the ionized gas by the microwave propagation and conversely small perturbations of the microwave propagation by the experimental cell containing the plasma. {"Effective" means weighted by $[1+(\nu/\omega_0)^2]^{-1}$, ω_0 being the microwave radian frequency.} The quantities $\langle\nu(t)\rangle$ and $\langle n_e^{\text{eff}}(t)\rangle$ are integrated on the whole volume of the ionized gas and it is shown in Sec. VI that they are weakly dependent on the non-Maxwellian electrons.

The interferometer has been described previously in the literature.[25,66] It allows measuring the phase shift $\langle\varphi(t)\rangle$ with an excellent time resolution (a few microseconds) (i) manually down to 1° with a precision of ±0.1°, or (ii) with two crystal detectors connected to a multichannel sampling device, from a few degrees to 10^{-3} deg.

The wave attenuation is also measured with an excellent time resolution and a precision of 0.1 dB using the interferometer. It is also deduced from the microwave power transmission through the ionized gas with a multichannel sampling analyzer. The attenuation $\langle A(t)\rangle$ is then determined down to 10^{-3} dB with good precision.

B. *X*-band microwave radiometry

The radiation temperature of the ionized gas has been measured as a function of time in the afterglow with a high sensitivity radiometer, previously described.[51,66] This reflection type, *X*-band, microwave radiometer has been designed according to the scheme described by Bekefi.[67] It directly gives the radiation temperature $\langle T_R(t)\rangle$ without the need for the knowledge of the absorptivity and reflectivity of the plasma branch. These two coefficients are only involved in the calculation of the precision of the measurements. Very careful calibration and control of the systematic errors by Monchicourt[51] along with the use of high-performance electronic components allowed the resolution of the radiation temperature to within 10 °K above 350 °K, for 20-μsec time resolution and integration time constants of approximately 100 sec. The electronic circuit including the detector, the monochannel sampling analyzer, and the lock-in amplifier has been constructed by Ahrweiller. At a given time in the afterglow the average radiation temperature $\langle T_R(t)\rangle$ depends on the spatial profiles of the electron concentration and electron energy, on the propagating microwave mode, and on the electron energy distribution function. We shall see in Sec. VI that the radiation temperature is strongly influenced by the non-Maxwellian electrons. Radiometry is an efficient means to show the existence of very energetic non-Maxwellian electron concentrations.

C. Mass spectrometry

The atomic- and molecular-ion currents at the wall of the discharge vessel have been measured with a quadrupole mass spectrometer through a very small hole (30 μm in diam, 10 μm long). A very careful calibration of the different transmission coefficients through the hole, the focusing electronics, and the quadrupole filter, along with the measurement of the electron multiplier gain allowed Lambert[68] to perform absolute ion-current measurements within a precision of 20% from

1 to 20 Torr for the atomic ions, and from 1 to 100 Torr for the molecular ions He_2^+.

A detailed description of the experimental device is to be published by Lambert and Cheret. The measured quantities at the wall, $Da_1\nabla n_1(t)$ and $Da_2\nabla n_2(t)$ are strongly dependent on the spatial distributions.

D. Optical absorption spectrometry

As has been pointed out (Figs. 1–3), the triplet atomic and molecular metastables play an important role during the helium afterglow in the electron energy balance and in the variation with time of the various particle concentrations. Their number densities have been deduced from the optical absorption measurements of the atomic lines 5015.7 and 3888.6 Å, corresponding to the transitions $3\,^1P \rightarrow 2\,^1S$ and $3\,^3P_{1,2} \rightarrow 2\,^3S$, and the rotational line 4649.4 Å, corresponding to the $Q3$ component of the molecular band $3p\,^3\Pi_g \rightarrow 2s\,^3\Sigma_u^+$. This optical absorption has been measured along the axis of the experimental cell in the small cylindrical volume (3.6 mm in diameter, 300.0 mm long) seen from the THR Jobin et Yvon monochromator. The sensitivity of the measurement has been considerably improved by the use of intense helium atomic and molecular sources of light built in collaboration with Professor D. E. Kerr and by the use of a very sensitive detection system: monochromator, photomultiplier, counting techniques, multichannel sampling analyzer, and online computer.

E. Optical emission spectrometry

The same optical system has been used to measure the decay with time of the atomic and molecular population densities of the excited states up to the principal quantum level $p = 18$,[69] from the relative intensity of the emitted light.

F. Determination of the spatial distributions

The radial distributions of the emitting molecules have been obtained, at different times in the afterglow, by Abel inversion. The radial profiles of the electron concentration have been deduced, the population densities of the excited molecular states being proportional to the square of the electron density for our experimental conditions.

The spatial distribution of the metastable concentrations have been measured at 40 Torr by optical absorption in a vertical plane including the axis of the cell through a series of ten 1-mm-diam diaphragms. These measurements, at different times in the afterglow, are long and difficult, very often at the limit of sensitivity of the optical detection. They have been performed for the atomic triplet metastable.[69]

VI. INTERPRETATION OF THE MEASUREMENTS

A. X-band microwave interferometry

As is well known,[65] the real part $\langle n_e^{\rm eff}(t)\rangle$ and the imaginary part $\langle (n_e\nu)^{\rm eff}(t)\rangle$ of the complex electrical conductivity of the ionized gas can be directly calculated from the measurements of $\langle A(t)\rangle$ and $\langle \varphi(t)\rangle$, as well as the average electron collision frequency $\langle \nu(t)\rangle = \langle (n_e\nu)^{\rm eff}(t)\rangle / \langle n_e^{\rm eff}(t)\rangle$. When the electron temperature cannot be considered as spatially uniform the electron collision frequency becomes a function of time and space even when the electron-ion collision frequency is negligible with regard to the electron-neutral collision frequency. $\nu_{ei}(v)$ is a function of $n_1(r,t)$, $n_2(r,t)$, and $T_e(r,t)$ (see Appendix); $\nu_{e0}(v)$ is constant for electron energies higher than 3 eV and otherwise proportional to v. The total collision frequency, weighted by $[1+\nu^2(v)/\omega_0^2]^{-1}$ and integrated on the electron energy, is then

$$\nu_{\omega_0}^{\rm eff}(r,t) = \frac{2}{3kn_e(r,t)T_e(r,t)} \times \left(\int_0^\infty \frac{\nu_{e0}(v)}{1+[\nu_{e0}(v)/\omega_0]^2} \tfrac{1}{2} m v^2 4\pi v^2 f_0(v)\,dv + \int_0^\infty \frac{\nu_{ei}(v)}{1+[\nu_{e0}(v)/\omega_0]^2} \tfrac{1}{2} m v^2 4\pi v^2 f_0(v)\,dv \right). \tag{53}$$

In this calculation we only neglect $[\nu_{ei}(v)/\omega_0]^2$ with respect to 1, which is always justified. If we integrate on the complete electron energy distribution function $f(v) = f_0(v) + f_1(v)$, the non-Maxwellian part $f_1(v)$ represents at the maximum a 2% increase of $\nu_{\omega_0}^{\rm eff}(r,t)$, for our experimental conditions.

At a given time, the real and imaginary parts of the complex conductivity cannot be simplified as has always been done previously assuming $\nu_{\omega_0}^{\rm eff}(r,t)$ is spatially uniform. They have been calculated from the following mathematical forms:

$$\langle (n_e\nu)^{\rm eff}(t)\rangle = \frac{\iint_{S'} |E(r,\theta)|^2 n_e(r,t)\nu_{\omega_0}^{\rm eff}(r,t) r\,dr\,d\theta}{\iint_S |E(r,\theta)|^2 r\,dr\,d\theta}, \tag{54}$$

where $E(r,\theta) = E_0 \cos[\pi r(\cos\theta)/2a]$ is the electric field of the propagating microwave mode, TE_{01}, in the waveguide, S' is the cross-sectional area of the discharge tube, and S is that of the waveguide, $(2a)^2$;

$$\langle n_e^{\mathrm{eff}}(t)\rangle = \frac{\iint_{S'} |E(r,\theta)|^2 \left[\int_0^\infty \{1/[1+(\nu_{e0}(v)/\omega_0)^2]\}^{\frac{1}{2}} m v^2 4\pi v^2 f_0(v)\, dv\right] r\, dr\, d\theta}{\iint_S |E(r,\theta)|^2 r\, dr\, d\theta}. \tag{55}$$

B. *X*-band microwave radiometry

At a given time in the afterglow, the average radiation temperature of the electrons in the experimental cell is measured by microwave radiometry. $\langle T_R(t)\rangle$ is averaged in each elementary volume on the electron energy distribution function $[f(v) = f_0(v) + f_1(v)]_{r,t}$. It also depends on the spatial profiles of the electron energy, electron concentration, elastic electron collision frequency, and on the propagating mode of the microwaves. The non-Maxwellian electrons have a high energy, and their contribution to the total radiation temperature is large, even if their number density is only 10^{-3} to 10^{-5} of the electron concentration.

The radiation temperature has been deduced from the theory of Wright and Bekefi.[70] At a microwave radian frequency ω_0, it is, for the Maxwellian electrons,

$$\langle T_e(t)\rangle_{\omega_0} = \frac{\iint_{S'} |E(r,\theta)|^2 n_e(r,t) T_e(r,t) \nu_{\omega_0}^{\mathrm{eff}}(r,t)\, r\, dr\, d\theta}{\iint_{S'} |E(r,\theta)|^2 n_e(r,t) \nu_{\omega_0}^{\mathrm{eff}}(r,t) r\, dr\, d\theta}, \tag{56}$$

and for the non-Maxwellian electrons,

$$\langle \Delta T_R(t)\rangle_{\omega_0} = \frac{\iint_{S'} |E(r,\theta)|^2 (2/3k) \left[\int_0^\infty \{\nu_{e0}(v)/[1+(\nu_{e0}(v)/\omega_0)^2]\}^{\frac{1}{2}} m v^2 4\pi v^2 f_1(v)\, dv\right] r\, dr\, d\theta}{\iint_{S'} |E(r,\theta)|^2 n_e(r,t) \nu_{\omega_0}^{\mathrm{eff}}(r,t) r\, dr\, d\theta}. \tag{57}$$

The elastic electron-ion collision frequency is negligible for high-energy electrons:

$$\langle T_R(t)\rangle_{\omega_0} = \langle T_e(t)\rangle_{\omega_0} + \langle \Delta T_R(t)\rangle_{\omega_0}.$$

It is then necessary to integrate on the frequency range $\Delta\omega = \omega_2 - \omega_1 = 1$ GHz of the radiometer:

$$\langle T_R(t)\rangle = \frac{1}{\omega_2 - \omega_1} \int_{\omega_1}^{\omega_2} \langle T_R(t)\rangle_\omega\, d\omega. \tag{58}$$

This calculated radiation temperature is directly compared to the measured values.

The resolution of our system of differential equations gives as a function of time and space the ion concentrations, electron density, electron temperature, and electron energy distribution function, which allow us to calculate the above average physical quantities [(53)–(57)].

C. Optical absorption measurements

The optical absorption measurements on the axis of the experimental cell, at a given wavelength, $a^\lambda(t)$, have to be interpreted in terms of absolute metastable concentrations.

(a) Atomic metastables. The oscillator strengths for the atomic transitions are well known. The gas temperature in the atomic source (3 Torr) is 700 ± 100 °K, determined from the rotational temperature of the $3p\,^3\pi_g$ level. Doppler line profiles have been taken for the emitted light of the atomic source.

(i) The singlet atomic metastables He($2\,^1S$) are very rapidly converted (23) into triplet atomic metastables. When the pressure is increased they become insignificant early in the afterglow, with regard to the concentrations of the main particles. They have only been measured at 5.0 and 10.0 Torr. At these low pressures Doppler absorption line profiles at 293 °K have been used. The corresponding metastable concentrations have been deduced from the theory of Mitchell and Zemansky.[71]

(ii) The triplet-atomic-metastable concentrations have been deduced from the calculations of Lambert[72] taking into account the fine structure[73,74] and the pressure broadening.

The pressure broadening is probably very small under our experimental conditions, and it has been estimated by extrapolation of previous measurements.[75–77] A consequence of the pressure broadening is to slow down the calculated decay of the triplet metastables during the early afterglow when the measured absorptions are large (above 50%).

(b) Molecular metastables. The oscillator strength of the observed transition has been calculated by Robben.[78] In the case of helium molecules the Bates and Damgaard theory[79] seems to be a good approximation. We have used their result, 0.119. The gas temperature in the molecular source (23 Torr) is 800 ± 100 °K, determined from the rotational temperature of the $3p\,^3\pi_g$ level. A Doppler profile has been assumed for the emitted rotational lines ($Q3$ component). We have not found any information on the pressure broadening of rotational lines in an ionized gas: The absorption line profile has also been assumed to be Gaussian. Anyway, because of the small absorption coefficients measured (less than 50%), an eventual pressure broadening would not modify the shape of the molecular metastable decay curves, but

would slightly increase the metastable $M_2(t)$ concentrations by a constant multiplier term.

The rotational temperature of the molecular metastable state has been found to be approximately 900 °K, by absorption techniques[69] at 40 Torr on two rotational lines $Q5$ and $Q7$. As these optical absorption measurements on several rotational lines, at different pressures and as a function of time, were much too long, we have accurately deduced the rotational temperature of the $3p\,^3\pi_g$ level by the emission, during the afterglow, of seven rotational lines $Q3$ to $Q15$. We have assumed that the rotational temperature of the lower state could not be much different from the rotational temperature of the upper state. At pressures less than 40 Torr, we obtain the same results as Kerr[12] and Callear and Hedges[80]: high "rotational temperatures," 550 °K at 5 and 10 Torr, and 660 °K at 20 Torr, independent of time during the first 2 msec. At higher pressures we observe a slow decay with time of the rotational temperature: from 700 to 560 °K at 40 Torr, 650 to 510 °K at 60 Torr, and 700 to 540 °K at 80 Torr, during the first 2 msec; and 750 to 430 °K at 100 Torr during the first 3 msec in the afterglow.

A 100 °K error on the rotational temperatures modifies the molecular metastable concentrations by 14%. The uncertainties on the gas temperature in the atomic and molecular light sources are negligible in the calculation of the metastable concentrations. The precision on the atomic metastables is always better than 15% for concentrations higher than 10^9 cm^{-3}. The uncertainty on the molecular metastable concentrations is less than 20% if we do not include the error bar on the oscillator strength.

VII. DESCRIPTION OF THE METHOD

A. Principle of the determination of the rate coefficients

Because of the couplings which have been presented above the rate coefficients of the various mechanisms cannot be separately determined. The method we have elaborated is based on a precise comparison between experimental results and calculations.

All the mechanisms which can occur in a helium afterglow at room temperature are first included in a system of coupled partial differential equations. The method we have developed to determine the set of coefficients of the differential equations lies in reproducing by computations all the experimental results obtained at several pressures, by varying the value of the unknown coefficients.

This method only applies when (a) the evolution with time of the physical quantities corresponding to *all the variables* of the system can be accurately measured and (b) the measured average physical quantities can be directly calculated from the computed values of the variables obtained as a function of time and space by the resolution of the coupled differential equations.

Therefore when the solution of the system of coupled partial differential equations allows us, at every given pressure between 5 and 100 Torr, to describe accurately all the measured experimental curves within the experimental error bars, over a wide dynamic range and *with the same set of rate coefficients and constants,* we conclude that (a) the afterglow is actually governed by the mechanisms taken into account, and (b) the rate coefficients are well determined with a precision which depends on the experimental uncertainties and on their respective influence on the shape of the computed curves at a given pressure.

This method cannot be expected to apply to the determination of the coefficients of only one partial differential equation, at only one pressure, because in this case, the solution may not be unique or, equivalently, a few coefficients may not be well determined. It also does not apply in the case of a system of coupled differential equations when the comparison of theory to experiment is only achieved at one pressure, for only one set of experimental values, although the probability of finding two different sets of rate coefficients reproducing the experimental curves is very small in this case. As a matter of fact, the couplings between the different terms of the coupled equations are strong, the asymptotic behavior of the curves, late in the afterglow are quite well known, and the variation range of a few coefficients has been bounded. But in this case a few coefficients will not be determined or will be obtained with a poor precision if their influence at the given pressure is negligible.

The method we have developed leads to a unique set of well-determined rate coefficients with the following conditions: (i) The same system of differential coupled equations allows the reproduction of all the experimental curves obtained in a large pressure range, from 5 to 100 Torr. (ii) At a given pressure all the experimental curves have to be well described by the system of differential equations, over a wide dynamic range during the afterglow. (iii) The measured and calculated average physical quantities have to be directly comparable.

B. Experimental conditions

The experimental techniques described in Sec. V have been applied at seven different pressures: 5.0, 10.0, 20.0, 40.0, 60.0, 80.0, and 100.0 Torr. At a given pressure all the diagnostics have been

rigorously used in the same discharge conditions, which is extremely important.

The pulse length was 51 μsec. The voltage pulse, current, and repetition rate were chosen, at every pressure, using the following criteria: (a) The discharge had to be well centered with a cylindrical symmetry of revolution. (b) The average current in the pulse had to be as weak as possible. (c) The decay rate of the ionizing pulse was required to be extremely fast, corresponding to negligible residual voltage by a time very early in the afterglow: The electron heating due to the residual electric field had to be less than 1 °K for measured radiation temperatures above 600 °K. (d) The repetition rate had to be as slow as possible, compatible with the stability of the plasma. (e) The reproducibility had to be excellent.

The precision of the measurements has been given in Secs. V and VI; the experimental error bars are indicated on the following figures. Before comparison with the computed curves a few checks have been done on the experimental data: (i) Late in the afterglow the exponential decay time constants measured as a function of pressure, for the microwave attenuation and phase shift, for the atomic- and molecular-ion currents, and for the molecular metastables were in good agreement with the previously published values. (ii) After the electrons have lost their excess energy to reach the gas temperature, the elastic electron-neutral collision frequency calculated from the measured average microwave attenuation and phase shift was in very good agreement with the theoretical values, integrated over space, and computed at every investigated pressure.

C. Computer program

The computer program written by Forge and Lieutaud (at C.I.S.I.) allows us, first, to solve the system of five coupled, partial differential equations in cylindrical coordinates with the same assumptions as in Sec. IV. The initial conditions are first given at time t_0 chosen in the afterglow at a given pressure. The variables $n_1(r,t)$, $n_2(r,t)$, $M_1(r,t)$, $M_2(r,t)$, $T_e(r,t)$, and $n_e(r,t)=n_1(r,t)+n_2(r,t)$ are calculated for a given set of coefficients in the field

$$0 \leq r \leq R, \quad t_0 \leq t \leq t_{\max}.$$

$t_{\max}$ in the computation is generally equal to four exponential decay time constants of the molecular ions. The precision of the computation does not increase when the number of steps in space is higher than 10. The width of steps in time is always calculated in order to take into account the fastest variation with time of the five variables.

(a) Initial conditions: The initial conditions at time t_0 chosen in the afterglow are (i) the initial values of the variables on the axis of the cell, $n_1(r=0,t_0)$, $n_2(r=0,t_0)$, $M_1(r=0,t_0)$, $M_2(r=0,t_0)$, and $T_e(r=0,t_0)$, and (ii) the initial spatial distributions of these five variables, normalized to 1 on the axis of the cell. The initial ion concentrations $n_1(r=0,t_0)$ and $n_2(r=0,t_0)$ are deduced from the measurements of the ion currents at the wall and the average effective electron density $\langle n_e^{\text{eff}}(r=0,t_0)\rangle$, assuming for each ion species a given spatial distribution, taken as the initial spatial profile. The initial metastable concentrations $M_1(r=0,t_0)$ and $M_2(r=0,t_0)$ are measured on the axis of the cell. Their spatial distributions at time t_0 are considered as a parameter of the system. The initial electron temperature on the axis of the cell $T_e(r=0,t_0)$ is calculated separately from $M_1(r=0,t_0)$, $M_2(r=0,t_0)$, $n_e(r=0,t_0)$, and the values chosen in this case for the γ and β coefficients. The spatial distribution of the electron temperature at time t_0 is also initially calculated from the spatial distributions taken for the atomic and molecular metastables at time t_0 and from the initial atomic- and molecular-ion profiles.

(b) Calculation of the average measured quantities. According to the *ab initio* assumptions to the imposed set of coefficients and according to the initial conditions, the computer program provides the calculated values of $n_1(r,t)$, $n_2(r,t)$, $M_1(r,t)$, $M_2(r,t)$, and $T_e(r,t)$. From these results the total, elastic, effective collision frequency $\nu_{\omega 0}^{\text{eff}}(r,t)$ is computed by integration over the Maxwellian electron energy distribution function (53), which is completely justified in this case. The exact electron energy distribution function is then calculated as a function of space at different times t_1 that were initially chosen.

Finally the average physical quantities directly comparable to the experimental values are calculated at different times t_1: The program first integrates the quantities $\langle (n_e\nu)^{\text{eff}}(t_1)\rangle$ (54) and $\langle n_e^{\text{eff}}(t_1)\rangle$ (55). The average attenuation $\langle A(t_1)\rangle$, phase shift $\langle \varphi(t_1)\rangle$, and elastic electron collision frequency $\langle \nu(t_1)\rangle$ are calculated from the preceding values of (54) and (55). The average radiation temperatures $\langle T_R(t_1)\rangle$ is then computed by the sum of formulas (56) and (57), integrated as in (58). Finally, the computer program provides the ion currents at the wall: $2D_1\nabla n_1(t_1)$ and $2D_2\nabla n_2(t_1)$.

(c) Comparison of theory to experiment. At a given pressure, the data provided to the computer are the set of rate coefficients, the initial conditions, and the experimental results as a function of time. The computed curves and the experimental points are displayed on a Benson plotter.

At a given pressure and for well-defined discharge conditions the following quantities are directly

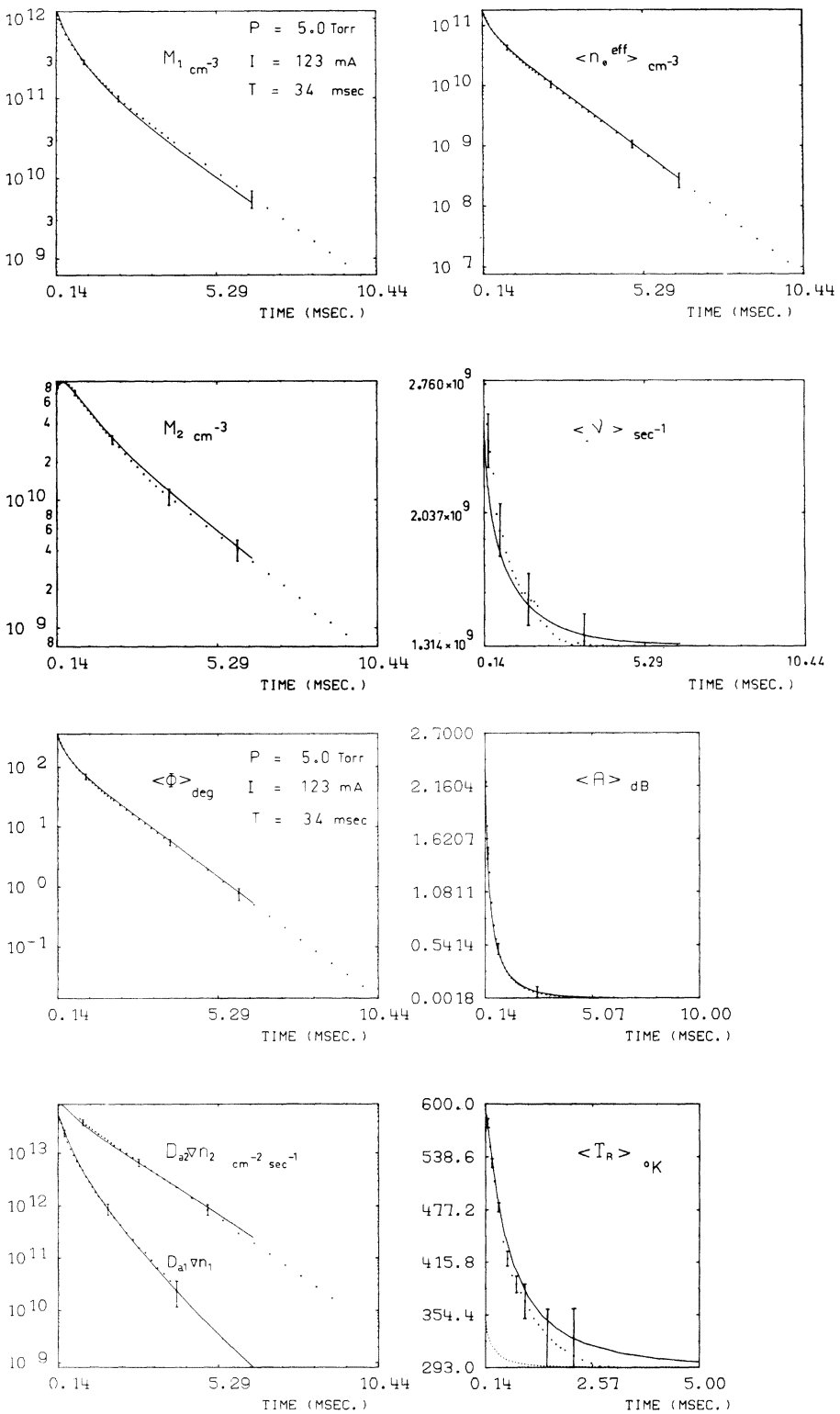

FIG. 5. Comparison of computed curves (full lines) to experimental points (dots) as a function of time, at 5.0 Torr, directly plotted by the computer. All these curves are calculated simultaneously. The lowest dotted curve on the radiation-temperature $\langle T_R(t)\rangle$ plot represents the average electron temperature.

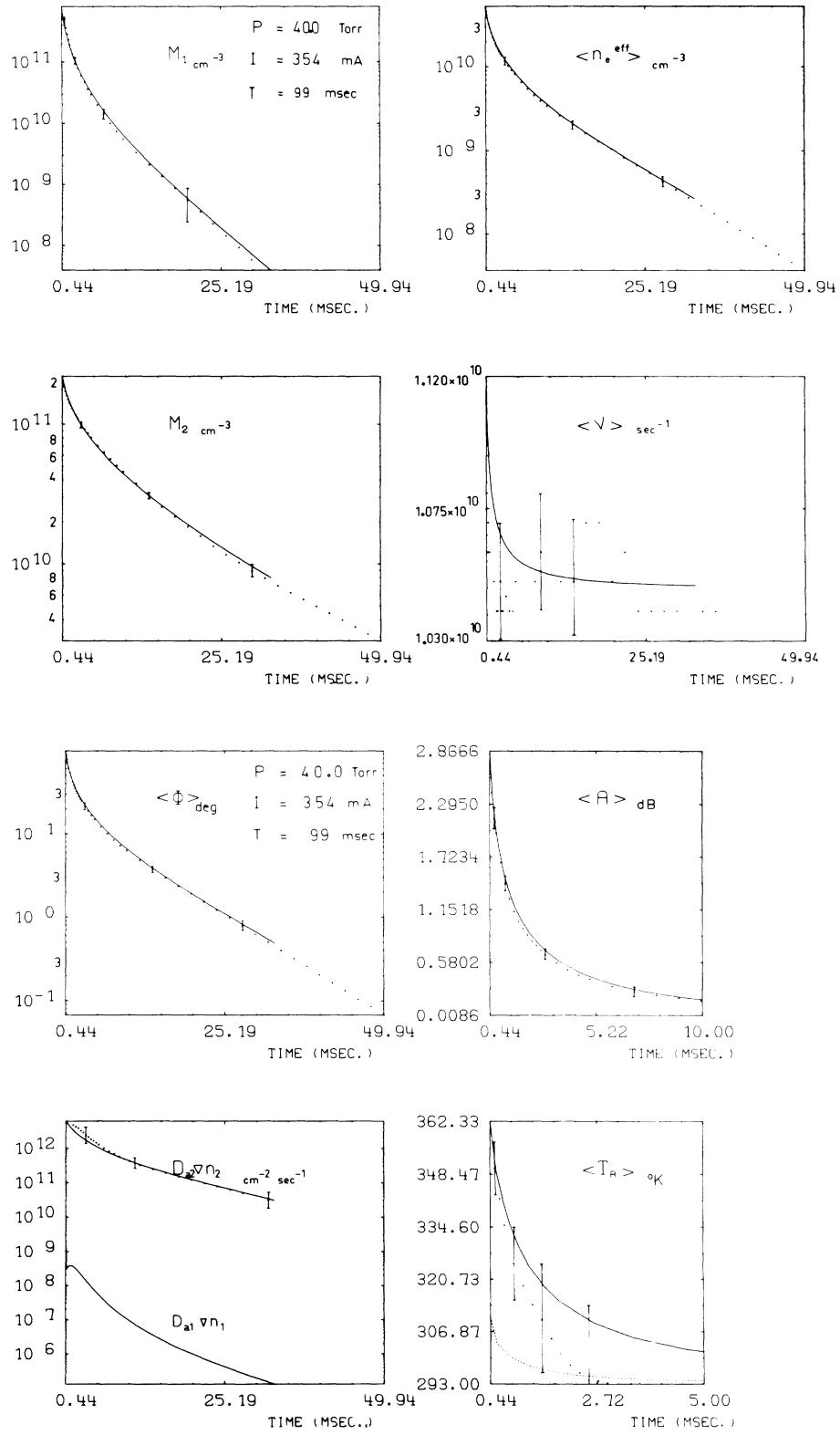

FIG. 6. Same comparisons as in Fig. 5, but at 40.0 Torr.

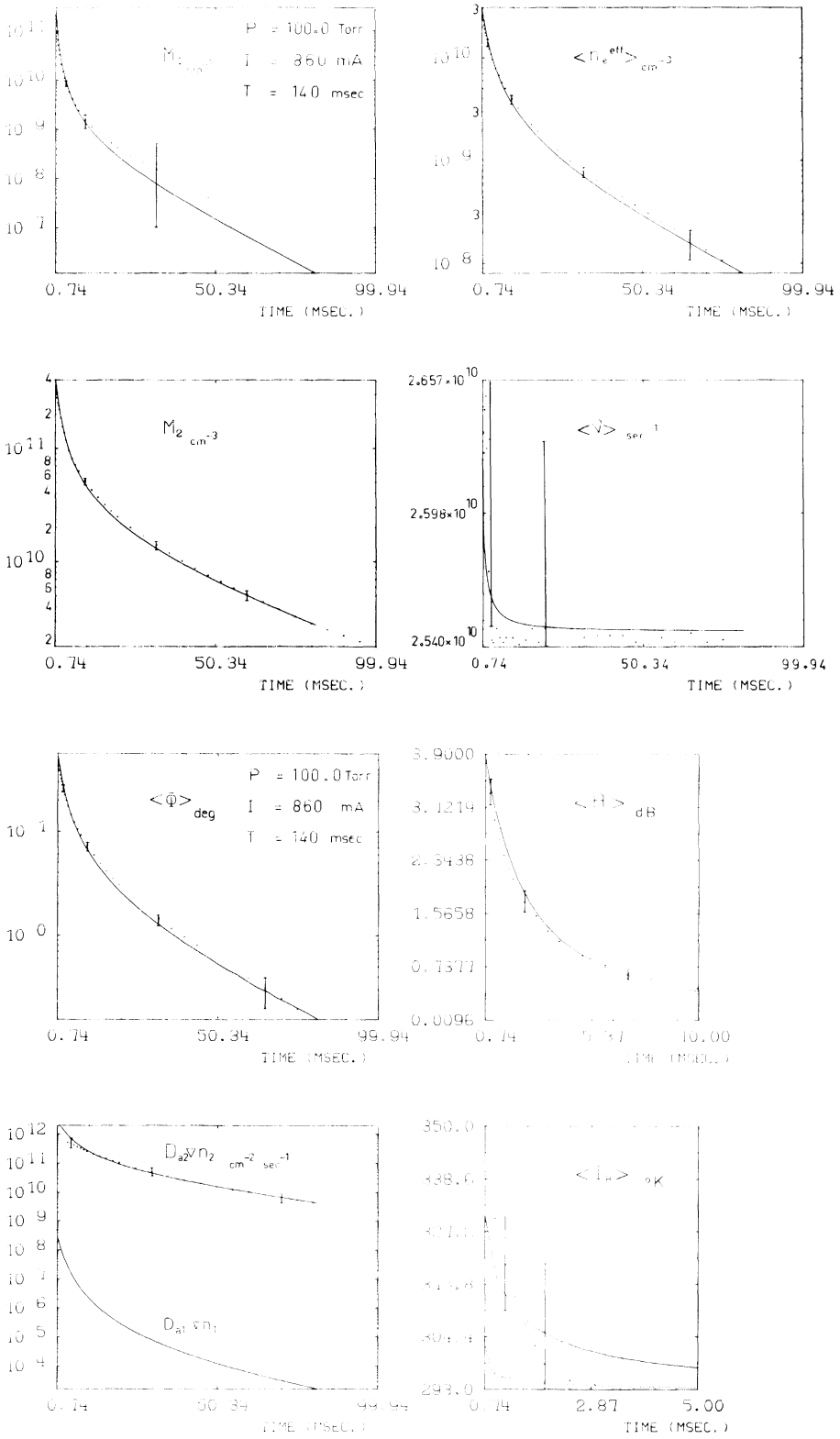

FIG. 7. Same comparisons as in Fig. 5, but at 100.0 Torr.

compared: (i) the variation with time of the atomic and molecular metastables calculated on the axis of the cell, $M_1(r=0,t)$ and $M_2(r=0,t)$, with the experimental results also measured on the axis of the cell; (ii) the computed curves of the microwave attentuation and phase shift with the corresponding measured values; (iii) the variation with time of the calculated average quantities (54) and (55) with the corresponding quantities directly deduced from the measurements of $\langle A(t)\rangle$ and $\langle\varphi(t)\rangle$; (iv) the computed elastic electron collision frequency $\langle\nu(t)\rangle$ with the corresponding value deduced from the measurements of $\langle A(t)\rangle$ and $\langle\varphi(t)\rangle$; (v) the evolution with time of the average radiation temperature $\langle T_R(t)\rangle$ (58) with the radiometric measurements; and (vi) the calculated atomic- and molecular-ion currents with the mass-spectrometric measurements.

It is a precise fit between *these nine computed curves and the corresponding measurements* which is simultaneously required at every investigated pressure. Only a few coefficients considered as parameters are varied in the program.

On the other hand the computed atomic- and molecular-ion concentrations on the axis of the cell, $n_1(r=0,t)$ and $n_2(r=0,t)$, are compared with the values deduced from the ion currents assuming a constant spatial distribution during the afterglow, such as a zero-order Bessel function. (The atomic- and molecular-ion concentrations cannot be measured on the axis of the experimental cell.) Contrary to the nine preceding comparisons this one is not "exact" but rather shows the influence of the variation with time of the spatial distributions on the shape of the ion-concentration decay curves.

In order to increase the precision in the determination of the rate coefficients and to take into account as well as possible the contribution of the spatial profiles we decided not only to reproduce theoretically the experimental data of the average effective electron concentrations $\langle n_e^{\text{eff}}(t)\rangle$ but also the experimental values of the average elastic electron collision frequency $\langle\nu(t)\rangle$ and we even decided to proceed to the calculation of the directly measured quantities $\langle A(t)\rangle$ and $\langle\varphi(t)\rangle$. As a matter of fact, if a good fit is obtained between these four computed curves and the experimental data it means that the assumption of a weak perturbation in the diagnostic by interferometry is satisfied and that the spatial distributions are well determined as a function of time by the computer program, the four preceding quantities being differently weighted by the spatial profiles of the various variables. On the other hand, the comparison of computed curves with $\langle A(t)\rangle$ and $\langle\varphi(t)\rangle$ directly obtained experimentally is more easily interpreted. The calculation of $\langle\nu(t)\rangle$ indicates the conditions where the elastic electron-ion collisions become negligible and shows the high sensitivity of this collision frequency to the measured values of $\langle A(t)\rangle$, which must necessarily be very accurate.

(d) Computed curves and experimental data. All the experimental data have been very well reproduced by the computer program at the seven investigated pressures with the same set of coefficients. Examples of data directly plotted by the computer are shown at 5.0, 40.0, and 100.0 Torr (Figs. 5–7).

In a first computation the initial conditions at every pressure have been chosen late enough in the afterglow (3 to 4 msec) that the electrons had reached the gas temperature: $T_e = T_g$. The system is then considerably simplified and is reduced to only four coupled partial differential equations. The initial concentrations of the charged particles and metastables are small and consequently the precision on a few coefficients is weak. The diffusion rates are quite well determined along with the coefficients β_{11}, β_{12}, β_{22}, δ, and k_{02}, which are correctly approximated. The rate coefficients depending on the electron density cannot be determined under these conditions. The initial conditions are then taken early in the afterglow (a few hundred μsec) where $T_e \neq T_g$. Only the following constants are assumed to be initially known: a, b_1, b_2, b_3, c_1, c_2, c_3, d_{11}, d_{12}, d_{22} (see Sec. IV). All the other coefficients are considered as parameters in the resolution of the system of differential equations, even when they are quite well known.

VIII. RESULTS

A. Reaction rate coefficients and constants (Table I)

1. Diffusion rate coefficients

The atomic and molecular diffusion rate coefficients for the ions He^+ and He_2^+ are found to be such that

$$D_{a1}p_0 = 410 \pm 10 \text{ cm}^2 \text{ Torr/sec},$$

$$D_{a2}p_0 = 640 \pm 20 \text{ cm}^2 \text{ Torr/sec},$$

with $p_0(\text{Torr}) = (273/293)P(\text{Torr})$, $T_g = 293 \pm 1\,^\circ\text{K}$, in good agreement with the previous published values,[5] and corresponding to the following reduced mobilities:

$$\mu_{01} = 10.4 \pm 0.3 \text{ cm}^2 \text{V}^{-1}/\text{sec},$$

$$\mu_{02} = 16.7 \pm 0.5 \text{ cm}^2 \text{V}^{-1}/\text{sec}.$$

The diffusion coefficient of the triplet atomic metastables is difficult to obtain, except at low gas pressure and low electron density, because of the

TABLE I. Comparison with previous results.

Da_1p_0	cm^2 Torr/sec	440 ± 9 [a]						410 ± 10 [v]
Da_2p_0	cm^2 Torr/sec	625 ± 5 [a]	675 ± 13 [b]	650 ± 8 [c]				640 ± 20 [v]
$D_{M1}p_0$	cm^2 Torr/sec	438 ± 23 [d]	455 ± 7 [b]					420 ± 10 [v]
$D_{M2}p_0$	cm^2 Torr/sec	289 ± 47 [d]	370 ± 35 [e]				300 [f]	305 ± 10 [v]
β_{11}	cm^3/sec	1.8×10^{-9} [g]	$(4.5 \pm 1.0) \times 10^{-9}$ [h]	$(1.7 \pm 0.3) \times 10^{-9}$ [i]	$*1.7 \times 10^{-9}$ [j]	$(2.2 \pm 0.2) \times 10^{-9}$ [k]	$(2.0 \pm 0.5) \times 10^{-9}$ [f]	$(1.5 \pm 0.3) \times 10^{-9}$ [v]
β_{12}	cm^3/sec					$(8 \pm 8) \times 10^{-10}$ [k]	$(2.5 \pm 1.0) \times 10^{-9}$ [f]	$(2.5 \pm 1.5) \times 10^{-9}$ [v]
β_{22}	cm^3/sec					$(3.8 \pm 0.5) \times 10^{-9}$ [k]	$(5 \pm 2) \times 10^{-10}$ [f]	$(1.5 \pm 0.5) \times 10^{-9}$ [v]
γ_1	cm^3/sec	$*2.2 \times 10^{-9}$ [l]	$*6.5 \times 10^{-10}$ [m]	$(4.5 \pm 1.0) \times 10^{-9}$ [h]	$*(2.9 \pm 0.1) \times 10^{-9}$ [o]		$(1.5 \pm 0.5) \times 10^{-10} T_e^{1/2}$ [f]	$(4.2 \pm 0.6) \times 10^{-9}$ [v]
γ_2	cm^3/sec					$(1.7 \pm 0.4) \times 10^{-9}$ [k]	$(9 \pm 2) \times 10^{-11} T_e^{1/2}$ [f]	$(3.8 \pm 0.8) \times 10^{-9}$ [v]
δ	$Torr^{-2}$/sec	0.26 ± 0.03 [d]	0.25 ± 0.01 [b]	0.35 [n]			0.20 [f]	0.20 ± 0.04 [v]
η	$Torr^{-2}$/sec	65 ± 15 [p]	67.7 [q]	85 ± 3 [a]				67 ± 5 [v]
χ_{11}		$*0.30$ [j]						0.30 ± 0.05 [v]
χ_{12}								$0 < \chi_{12} < 0.3$ [v]
χ_{22}								$0 < \chi_{22} < 0.3$ [v]
k_{02}	cm^6/sec	$(2.0 \pm 0.5) \times 10^{-27}$ [r]	0 [s]	1.25×10^{-26} [t]				$(5 \pm 1) \times 10^{-27}$ [v]
k_{e2}	cm^6/sec	$(2.0 \pm 0.7) \times 10^{-20}$ [r]	2×10^{-20} [s]	0 [t]				$(4.0 \pm 0.5) \times 10^{-20}$ [v]
α_{c2}	cm^3/sec	$\sim 5 \times 10^{-10}$ [r]	3.5×10^{-9} [s]	1.1×10^{-8} [t]				$< 5 \times 10^{-10}$ [v]
x_2						$\alpha_2 = 3 \times 10^{-18} \times n_e^{0.814}$ cm^3/sec at 1.86 Torr [k]		1 ± 1 [v]
y_2								4.0 ± 0.5 [v]
k_{01}	cm^6/sec							0 [v]
k_{e1}	cm^6/sec					$(7.6 \pm 0.5) \times 10^{-20}$ [u]		$(6 \pm 2) \times 10^{-20}$ [v]
α_{c1}	cm^3/sec							0 [v]
y_1						4.4 ± 0.1 [u]		4.0 ± 0.5 [v]
k_{11}				$0.7 < k_{11} \leq 1$ [h]		0.75 ± 0.2 [k]		1.0 [v]
k_{21}				$0.7 < k_{21} + k_{22} \leq 1$ [h]			0.70 [f]	0.70 ± 0.05 [v]
k_{22}						$0.5 \leq k_{22} \leq 0.9$ [k]		0.20 to 0 [v]

[a] See Ref. 5.
[b] See Ref. 81.
[c] See Ref. 12.
[d] See Ref. 7.
[e] See Ref. 83.
[f] See Ref. 82.
[g] See Ref. 38.
[h] See Refs. 46 and 88.
[i] See Ref. 56.
[j] See Ref. 47.
[k] See Ref. 84.
[l] See Ref. 52.
[m] See Ref. 48.
[n] See Ref. 91.
[o] See Ref. 53.
[p] See Ref. 3.
[q] See Ref. 14.
[r] See Ref. 25.
[s] See Ref. 31.
[t] See Ref. 30.
[u] See Ref. 16.
[v] This work.
* Theoretical works.

production terms due to electron-ion recombination [(4)–(22)] and because of the metastable conversion term (24). We find

$$D_{M_1} p_0 = 420 \pm 10 \text{ cm}^2 \text{ Torr/sec},$$

in good agreement with Phelps's published value,[7] 438 ± 23 at $T_g = 293$ °K, but less than the value given by Huggins and Cahn,[81] 455 ± 7 at the same gas temperature.

The diffusion rate coefficient of the molecular metastables is much easier to determine because of the fast decay of the atomic metastables at pressures above 20 Torr and because of the very small production term due to the recombination. We find the same coefficient as previously published by our group,[82]

$$D_{M_2} p_0 = 305 \pm 10 \text{ cm}^2 \text{ Torr/sec},$$

in good agreement with Phelps's value,[7] 289 ± 47 at 293 °K, but about 20% less than the value published by Gusinow *et al.*,[83] 370 ± 35, measured with a channeltron at pressures between 2.7 and 20 Torr, where the triplet-atomic-metastable concentrations are not low enough to be neglected.

2. *Metastable-metastable ionization rate coefficients*

(a) Collisions between triplet atomic metastables. We have obtained

$$\beta_{11} = (1.5 \pm 0.3) \times 10^{-9} \text{ cm}^3/\text{sec},$$

in excellent agreement with the first measurements by Phelps and Molnar,[38] and with the more recent value published by Castell and Biondi,[57] $(1.7 \pm 0.3) \times 10^{-9}$ cm^3/sec, and with the recent calculations of Garrison *et al.*,[47] who found 1.7×10^{-9} cm^3/sec as an upper limit at 300 °K. We previously obtained[82] $(2.0 \pm 0.5) \times 10^{-9}$ with a much simpler model.

Theoretical calculations of Bates *et al.*[48] gave 6.2×10^{-10} cm^3/sec at 293 °K.

Collins *et al.*[84] found $(2.2 \pm 0.2) \times 10^{-9}$ cm^3/sec at 1.86 Torr, 50% higher than our result. Finally Johnson and Gerardo[46] published $\beta_{11} = (4.5 \pm 1.0) \times 10^{-9}$ cm^3/sec; this large value is discussed in Sec. IX.

(b) Collision between two molecular metastables. We find for the corresponding rate coefficients β_{22} the same value as for β_{11} with a lower precision:

$$\beta_{22} = (1.5 \pm 0.5) \times 10^{-9} \text{ cm}^3/\text{sec}.$$

All the possible systematic uncertainties (oscillator strength, temperatures, pressure broadening) lead to an eventual modification of the absolute values of $M_2(t)$ but conserve the shape of the experimental curves and therefore have a weak influence on the value of β_{22}.

The only other results to compare with are a value published by Collins *et al.*[84] which is 2.5 times larger, $(3.85 \pm 0.5) \times 10^{-9}$ cm^3/sec, but only obtained at one pressure, 1.86 Torr, where the molecular metastables do not play a dominant role, and a value we have published[82] which is three times too small. Three main reasons can explain this discrepancy: (i) We only solved in Ref. 82 the continuity equations of the atomic and molecular metastables. (ii) Each equation was considered separately and we did not take into account the spatial distributions. (iii) Only two pressures, 7 and 40 Torr, had been investigated and the recombination rate coefficients used[25] were too small, the more so as the electron temperature was overestimated.

(c) Collision between atomic and molecular metastables. Although the β_{12} coefficient arises in the five coupled differential equations it remains difficult to determine with accuracy, for it scarcely appears in a predominant term except at high pressure and early in the afterglow where the concentrations of atomic and molecular metastables are important. We have found

$$\beta_{12} = (2.5 \pm 1.5) \times 10^{-9} \text{ cm}^3/\text{sec};$$

we previously published the same value,[82] which is surprisingly larger than β_{11} or β_{22}. Collins *et al.*[84] found $(8 \pm 8) \times 10^{-10}$ cm^3/sec at 1.86 Torr.

3. *Electron-metastable rate coefficients*

We cannot separate in this model the collisional excitation rates from the superelastic deexcitation rate of the metastables. But we have seen that for our experimental conditions the superelastic collisions are much more probable, especially for the atomic metastables.

(a) Collisions between electrons and triplet atomic metastables. The classical value calculated by Gryzinsky[52] was 2.2×10^{-9} cm^3/sec independent of T_e for the superelastic collision rate coefficient γ_1. Bates *et al.*[48] gave $3.8 \times 10^{-11} T_e^{0.5}$ cm^3/sec for $T_e < 1500$ °K. More recently Nesbet *et al.*[53] calculated $\gamma_1 = 2.9 \times 10^{-9}$ cm^3/sec, independent of T_e, 4.5 times the value of Bates at room temperature.

We find

$$\gamma_1 = (4.2 \pm 0.6) \times 10^{-9} \text{ cm}^3/\text{sec},$$

with $z_1 = 0$, which means independent of T_e. This destruction rate coefficient of the atomic metastables is of course efficient at low gas pressure, but also plays an important role at high pressure early in the afterglow, in the decay of $M_1(t)$ and as a source term for the radiation temperature. It can then be precisely determined. We previously found[82] $\gamma_1 = 1.5 \times 10^{-10} T_e^{0.5}$, which in the early

afterglow, when these processes are predominant, gives approximately the same value, T_e being overestimated.

(b) Collisions between electrons and molecular metastables. This mechanism is an important destruction term at every pressure. We obtain

$$\gamma_2 = (3.8 \pm 0.8) \times 10^{-9} \text{ cm}^3/\text{sec}.$$

This coefficient is found to be independent of the electron temperature: $z_2 = 0$. It is 2.2 times larger than the value given by Collins *et al.*[84] obtained at 1.86 Torr. The same remark as above applies for the rate coefficient $\gamma_2 = 9 \times 10^{-11} T_e^{0.5}$, we found previously.[82]

4. Metastable conversion rate coefficient

The conversion of atomic metastables into molecular metastables depending on P^2 is not important at low gas pressure. It begins to play a role above 20 Torr. At high pressure the conversion is an important term only in the very early afterglow, because $M_1(t)$ is decaying very fast, but $\delta P^2 M_1$ still plays a determinant role.

Between 20.0 and 100.0 Torr we find

$$\delta = 0.20 \pm 0.04 \text{ Torr}^{-2}/\text{sec}.$$

This result is 23% less than Phelps's value[7] and 20% less than Huggins and Cahn's.[81] Jardino *et al.*[82] gave the same result.

5. Ion conversion rate coefficient

The three-body conversion of atomic ions into molecular ions He_2^+ is always the dominant term of the continuity equation of $n_1(t)$, even at 5 Torr. We obtain the same value as Phelps and Brown[3] and Gerber *et al.*,[14]

$$\eta = 67 \pm 5 \text{ Torr}^{-2}/\text{sec}.$$

6. Recombination of electrons with molecular ions He_2^+

(a) The recombination rate α_2 is pressure dependent. Qualitatively we confirm the influence, shown for the first time in our laboratory,[25] of the inelastic collisions between neutral particles on the value of the electron-ion recombination rate coefficient α_2.

Quantitatively the neutral-stabilized rate coefficient k_{02} is 2.5 times larger than the value we published previously,[25] where the electron temperature was assumed to be constant and equal to 300 °K and the collisions between metastables were neglected. We find

$$k_{02} = (5 \pm 1) \times 10^{-27} \text{ cm}^6/\text{sec}.$$

This value is 2.5 times smaller than the result obtained by Johnson and Gerardo.[30] Boulmer *et al.*[31] did not see any pressure dependence between 20 and 30 Torr. They concluded $k_{02} = 0$.

(b) α_2 depends on electron concentration. Here again we confirm the qualitative results obtained previously.[25] The electron-stabilized recombination term $k_{e2} n_e$ is absolutely necessary not only to describe the experimental data at low pressure, but also to reproduce the measurements of $\langle n_e^{\text{eff}}(t) \rangle$, for instance, at 80 and 100 Torr in the early afterglow. As a matter of fact the atomic and molecular metastables, at these high pressures and very early in the afterglow, are so important that the source term of electrons leads to high concentrations of electrons which experimentally decay very fast. This behavior cannot be described without a strong electron density dependence of α_2:

$$k_{e2} = (4.0 \pm 0.5) \times 10^{-20} \text{ cm}^6/\text{sec}.$$

This coefficient is twice our previous value[25] without taking into account the effect of metastables. This value was confirmed later on by Boulmer *et al.*[31] Johnson and Gerardo[30] claimed α_2 does not depend on electron density and therefore that $k_{e2} = 0$. Their arguments will be discussed in Sec. IX.

(c) Constant part of the recombination rate coefficient α_2. This constant term is very small and always negligible with respect to the sum of the two other recombination terms, $k_{e2} n_e + k_{02} n_0$. It can be included in the error bars of the sum of these two terms in our experimental conditions. Its upper limit is 5×10^{-10} cm^3/sec, in complete disagreement with the value of 1.1×10^{-8} cm^3/sec given by Johnson and Gerardo[30] and the result of Boulmer *et al.*[31] of 3.5×10^{-9} cm^3/sec.

(d) Electron temperature dependence of α_2. In order to simplify the formulation and the use of the system of differential equations we have assumed that for our experimental conditions, when the electron-stabilized recombination is dominant, its electron temperature dependence y_2 does not vary with the electron density. The value of y_2 has to be determined at low gas pressure, high electron density, and high electron temperature: 10 and 20 Torr. (The electron temperature is too small at 5 Torr because of the free diffusion of the energetic electrons.) We found

$$y_2 = 4.0 \pm 0.5.$$

It is more difficult to determine precisely the electron temperature dependence x_2 of the neutral-stabilized part of the electron-He_2^+ recombination. Conditions of high neutral concentration, high electron temperature, and low electron density are required. The upper limit of x_2 is equal to 2.

$$x_2 = 1 \pm 1.$$

7. Recombination of electrons with atomic ions He^+

The atomic-ion concentration decreases very fast during the afterglow under our experimental conditions. The dominant term corresponds to the conversion process giving molecular ions, even at 5 Torr. Under these conditions it is quite difficult to get good precision for the electron-ion recombination rate coefficient α_1. We have first used the formula given in Ref. 16:

$$\alpha_1 = \frac{8.1\times10^{-20}}{1+0.079P}\left(\frac{T_e(r,t)}{T_g}\right)^{-4.4} n_e(r,t)\,.$$

The diffusion, conversion, and production terms of atomic ions being determined, we have tried to fit the experimental atomic-ion current curves, obtained at 5, 10, and 20 Torr, varying the coefficients of the more general form used for the electron-ion recombination coefficient. We find

$$k_{e1} = (6\pm2)\times10^{-20}\ \mathrm{cm^6/sec}\,,$$

$$k_{01} = 0\,,\quad \alpha_{c1} = 0\,,$$

$$y_1 = 4.0\pm0.5\,,$$

in good agreement with the coefficients obtained in Ref. 16. Better precision could be reached at lower gas pressure. $k_{01}=0$ means that associative ionization (4) is negligible, as well as processes (7) and (10).

8. Production of metastables due to recombination

(a) Recombination of atomic ions. All the recombined atomic ions give $He(2\,^3S)$ directly or after singlet to triplet conversion.

$$k_{11} = 1\,.$$

Collins *et al.*[84] give 0.75 ± 0.2. $k_{11}=1$ also shows associative ionization (4) is negligible.

(b) Recombination of molecular ions. At every pressure investigated 70% of the recombined molecular ions provide atomic metastables $He(2\,^3S)$.

$$k_{21} = 0.70\pm0.05\,.$$

Cheret and Lambert[85] first showed this strong production of atomic metastables due to electron-ion recombination of He_2^+. The proportion of recombined molecular ions producing molecular metastables decreases with increasing pressure.

$$k_{22} = 0.20\pm0.05 \quad \text{at 5 Torr}\,,$$
$$= 0.10\pm0.05 \quad \text{at 20 Torr}\,,$$
$$= 0.05\pm0.05 \quad \text{at 40 Torr}\,,$$
$$= 0 \quad \text{above 40 Torr}\,.$$

At 1.86 Torr, Pitchford *et al.*[84] give

$$0.5 \leq k_{22} \leq 0.9\,.$$

Johnson and Gerardo[46] give the total fraction of recombination events resulting in metastable species (atomic and molecular metastables), $0.7 < k_{21} + k_{22} \leq 1$. We find

$$k_{21} + k_{22} = 0.90 \quad \text{at 5 Torr}$$
$$= 0.70 \quad \text{above 40 Torr}\,.$$

9. Percentage of atomic ions produced in collisions between metastables

These fractions have to be determined at low gas pressure, from the atomic-ion concentrations. At $1 \leq P \leq 5$ Torr the atomic metastables are dominant; 30% of ionizing collisions between atomic metastables give atomic ions (27);

$$\chi_{11} = 0.30\pm0.05\,,$$

in excellent agreement with the theoretical results of Garrison *et al.*[47]

At 10 and 20 Torr the molecular-metastable concentrations become predominant early in the afterglow, but the precision on the measured atomic-ion concentrations is not good enough to give the corresponding coefficients χ_{12} and χ_{22}. We only know that if we impose $\chi_{12}=\chi_{22}=\chi_{11}=0.3$, the production term of atomic ions increases too fast in the afterglow with respect to the experimental results:

$$0 < \chi_{12} < 0.3\,,\quad 0 < \chi_{22} < 0.3\,.$$

10. Vibrational relaxation of molecular ions

The vibrational relaxation of molecular ions (15) increases the energy of the Maxwellian electrons, but does not modify the high-energy tail of the electron energy distribution function. The influence of the electron temperature $\langle T_e(t)\rangle$ on the measured radiation temperature $\langle T_R(t)\rangle$ is small except in the very early afterglow. The heating term taken into account only refers to process (1) and underestimates the total vibrational relaxation mechanism (15). Consequently it has not been possible to estimate the coefficient μ. We have taken $\mu=1$. To get better precision on this heating process it would be necessary to measure directly the electron temperature. We can only refer to the calculated elastic electron collision frequency, which is sensitive to the electron temperature in the early afterglow at 5 Torr and is well reproduced by taking $\mu=1$. However, the sensitivity of the calculated electron temperature to the variation of this parameter is not sufficient to conclude the vibrational relaxation of the molecular ions has been experimentally shown. Further measurements are necessary.

B. Spatial distributions

The spatial profiles of the five variables considered interact during the afterglow and influence the average values of the measured physical quantities, more especially the interferometric, radiometric, and mass-spectrometric experimental results. These spatial distributions vary with time and strongly depend on one another and upon the nature of the dominant mechanisms. Their influence is particularly sensitive to the local electron energy distribution functions and on the atomic- and molecular-ion currents. A general characteristic of all these spatial distributions is to broaden in the early afterglow under the influence of nonlinear terms and slowly return later to a zero-order Bessel function $J_0(r)$ for $n_e(r,t), n_2(r,t)$, and $M_2(r,t)$ or to approximate the square of a zero-order Bessel function $J_0^2(r)$ for $n_1(r,t)$ and $M_1(r,t)$. The nonlinear terms βM^2 and $k\alpha n_e^2$ prevail over the diffusion rates for these two atomic species, in the later afterglow.

The measured intensity of the emitted band $3p\,^3\pi_g \rightarrow 2s\,^3\Sigma_u^+$, which is proportional to the square of the electron density at pressures above 5 Torr, shows that the spatial profile of $n_e(t)$ is never very different from a zero-order Bessel function. The same behavior can be expected for molecular ions. The spatial distribution of the atomic ions at a given time in the afterglow can then be deduced from the measured ion currents at the wall and from the average electron density.

The computer program shows very rapidly whether the spatial profiles initially given are compatible with one another. For instance, if either a uniform distribution or a very pinched profile are initially imposed for one of the five variables, the program gives, in these two limiting cases and in a few tens of μsec, the same calculated spatial distributions, except when this test is applied to $M_1(t)$, which is influenced by the initial conditions for a longer period of time. This very fast self-consistent rearrangement, observed at every pressure investigated and for every variable except $M_1(t)$, towards a set of compatible spatial distributions is a very important information source, well illustrated by the behavior of the calculated spatial distribution of $T_e(t)$ at 20 Torr, and shown in Fig. 8. The atomic metastable concentration is measured on the axis of the cell. Its spatial distribution plays an important role in the radiation temperature in the early afterglow and in the decay as a function of time of the atomic metastables $M_1(r,t)$. Therefore it has been well determined and is in satisfactory agreement with the measurements of Jardino[69] at 40 Torr.

Two other examples allow the illustration of the importance of the spatial distributions:

(a) At every pressure investigated a good fit has been obtained between theory and experiment on the *average quantities*, which are directly comparable, such as $\langle n_e^{\text{eff}}(t)\rangle$, $\langle A(t)\rangle$, $\langle \varphi(t)\rangle$, $\langle \nu(t)\rangle$, $D_{a_2}\nabla n_2(t)$, and $D_{a_1}\nabla n_1(t)$. On the other hand, the computed curves for the atomic and molecular ions *on the axis of the cell*, $n_1(r=0,t)$ and $n_2(r=0,t)$, do not coincide with the corresponding curves deduced from the experimental results assuming a constant spatial distribution, as shown on Figs. 9(a) and 9(b) at 10 and 20 Torr.

(b) The ion currents at the wall are doubly sensitive to the spatial distributions. The initial very fast decay and the bump experimentally observed on the atomic-ion currents at 10 and 20 Torr were first interpreted *a priori* as an apparatus effect, but later were shown to have been very well reproduced in fact by varying the initial spatial profile of $n_1(r,t)$ [Figs. 9(a) and 9(b)]. The fast

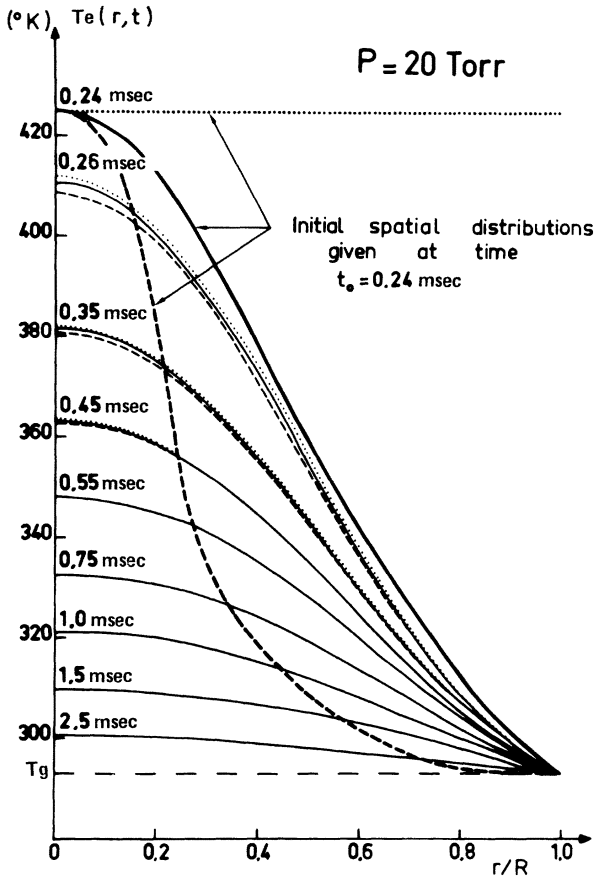

FIG. 8. Spatial profiles of the electron temperature $T_e(r,t)$ as functions of time in the afterglow, at 20.0 Torr, for various initial conditions. A very fast (less than 20 μsec) self-consistent rearrangement of the spatial distributions is observed.

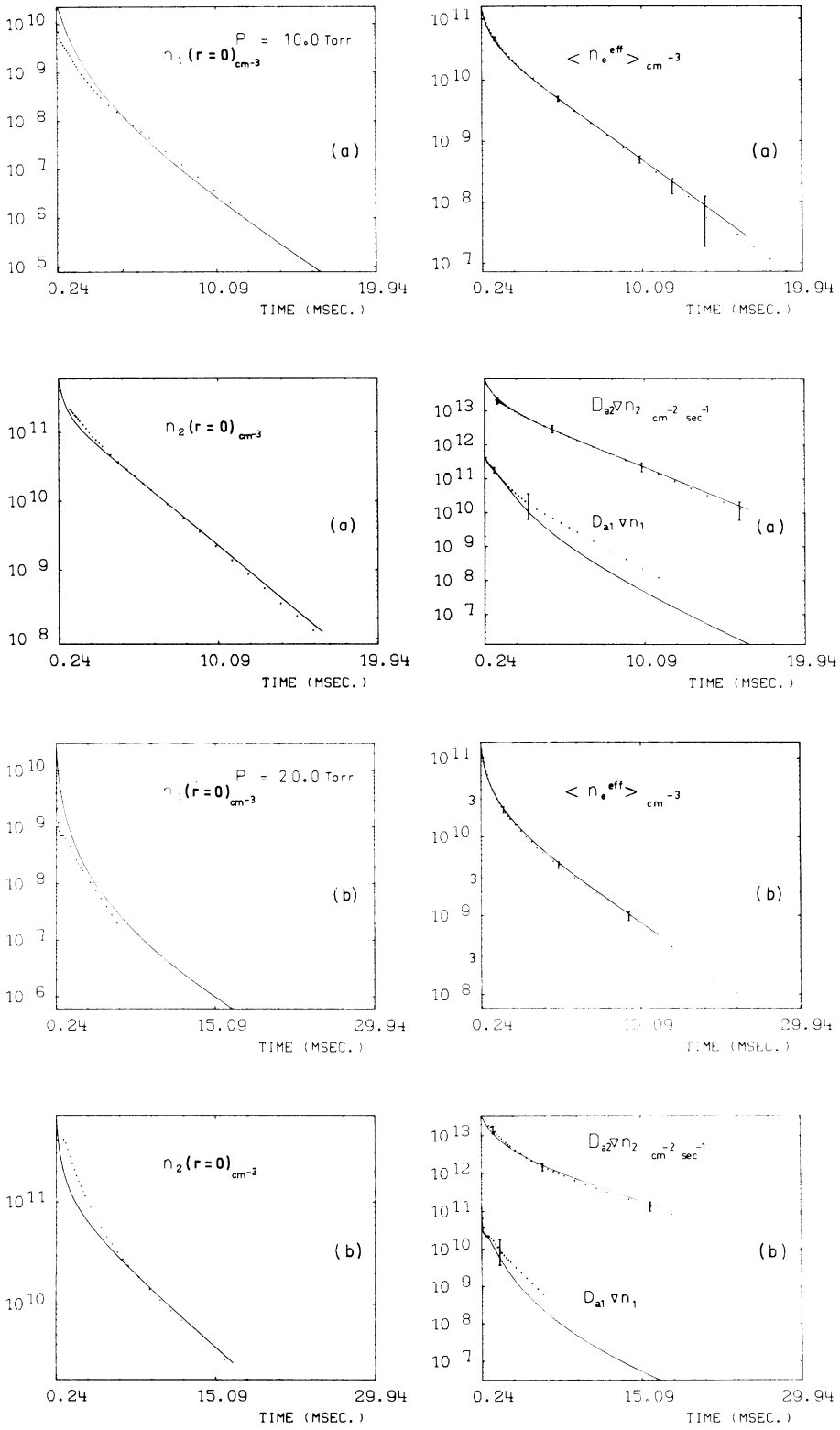

FIG. 9. Influence of the spatial distributions at (a) 10.0 Torr and (b) 20.0 Torr.

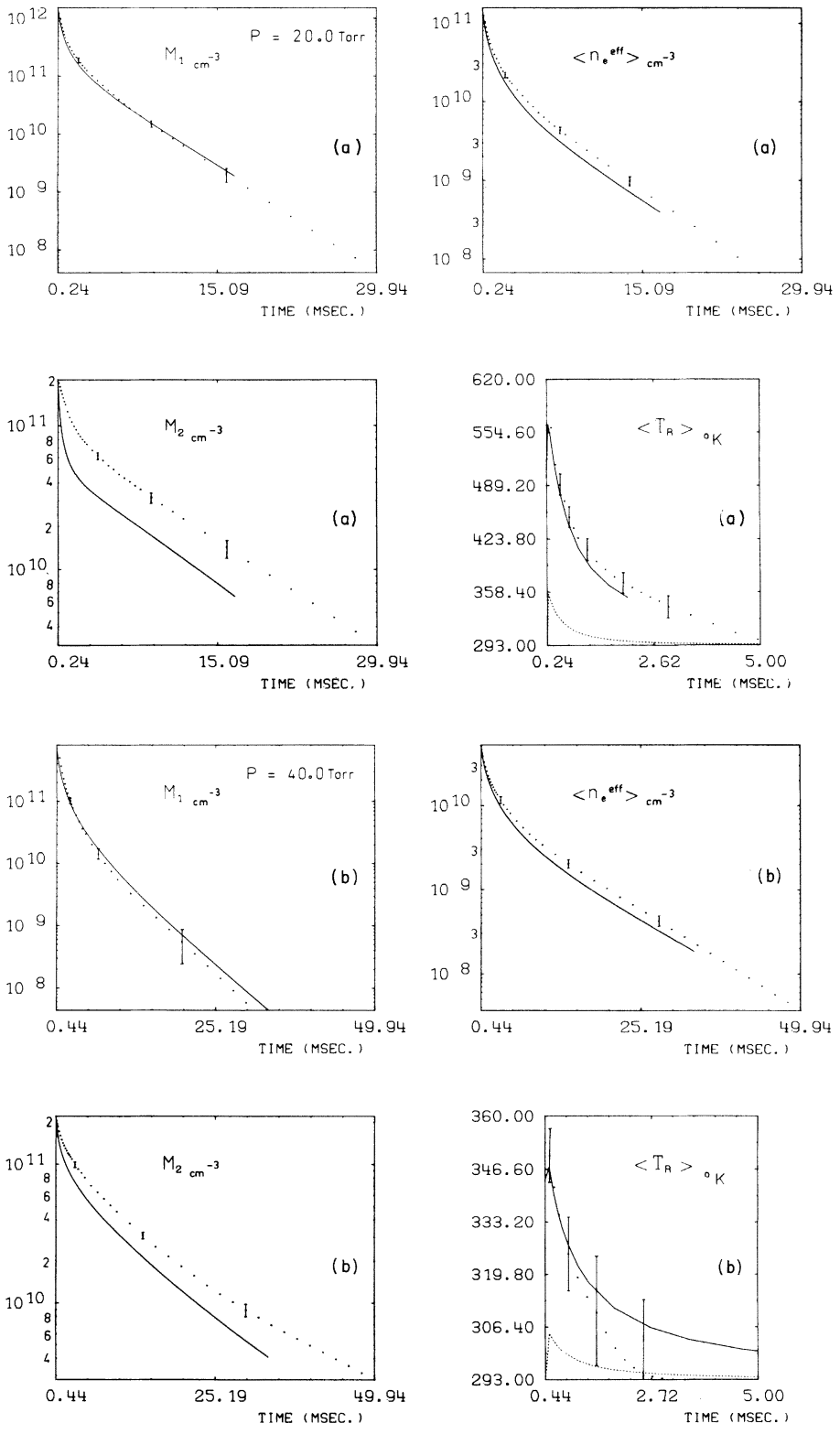

FIG. 10. Comparison with our experimental data of computed curves (full lines) using the Johnson and Gerardo coefficients at (a) 20.0 Torr and (b) 40.0 Torr.

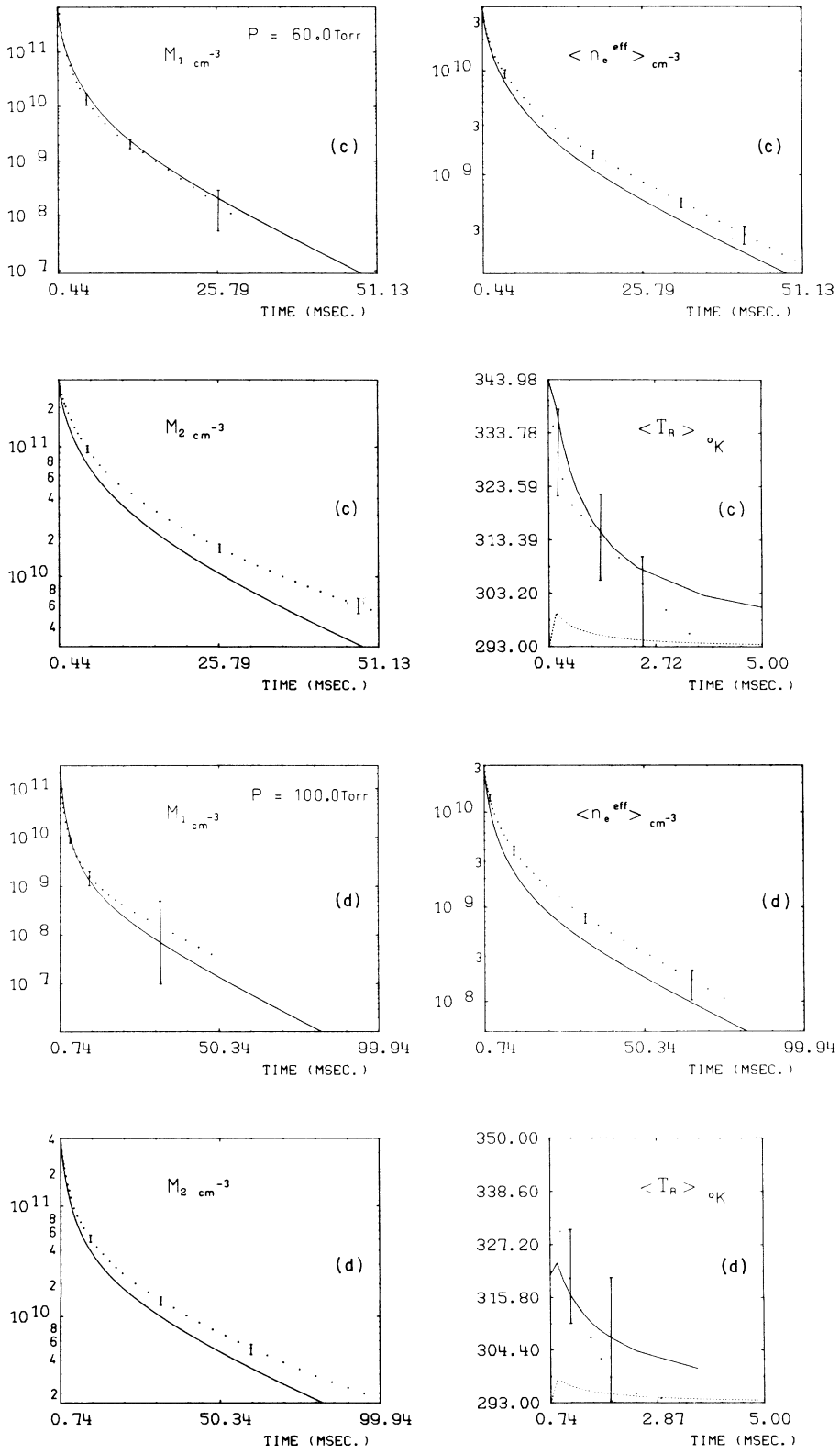

FIG. 10. *(continued)* (c) 60.0 Torr and (d) 100.0 Torr.

variation of this current is due to the evolution of the spatial distributions.

C. Comparison with previous experimental results

We wanted to use our computer program with the set of rate coefficients and constants we obtained to reproduce the experimental results previously published. Unfortunately we did not find in the literature any complete set of experimental data, measured at a given pressure and exactly with the same discharge conditions, which could be modeled by our computer program. As a matter of fact we need the experimental decay curves of the various quantities which can be calculated and also a considerable amount of information on the characteristics of the diagnostics, on the geometry of the experimental cell, etc.

The published experimental data being much too limited, we decided to apply the published sets of coefficients to our model and to compare the theoretical results with our measurements. We first used the coefficients published by Johnson and Gerardo[30,46] for the interpretation of our measurements [Figs. 10(a)–10(d)]. They assumed the electron temperature was constant and equal to T_g; we imposed as initial conditions $T_g = 293$ °K. We used all their coefficients as published,

$$\beta_{11} = \beta_{12} = \beta_{22} = 4.5 \times 10^{-9} \text{ cm}^3/\text{sec},$$

$$\gamma_1 = \gamma_2 = 4.3 \times 10^{-10} \text{ cm}^3/\text{sec},$$

$$\eta = 67.8 \text{ Torr}^{-2}/\text{sec},$$

$$\delta = 0.26 \text{ Torr}^{-2}/\text{sec},$$

$$k_{e2} = 0,$$

$$k_{02} = 1.25 \times 10^{-26} \text{ cm}^6/\text{sec},$$

$$\alpha_{c2} = 1.1 \times 10^{-8} \text{ cm}^3/\text{sec},$$

$$k_{21} = 0.7,$$

$$D_{a_1} p_0 = 410 \text{ cm}^2 \text{ Torr/sec},$$

$$D_{a_2} p_0 = 640 \text{ cm}^2 \text{ Torr/sec},$$

$$D_{M_1} p_0 = 445 \text{ cm}^2 \text{ Torr/sec},$$

$$D_{M_2} p_0 = 370 \text{ cm}^2 \text{ Torr/sec},$$

At 20 Torr, Fig. 10(a) shows a satisfactory agreement for $M_1(r=0, t)$ during the whole afterglow and for $\langle n_e^{\text{eff}}(t) \rangle$ during 1 or 2 msec, using the Johnson and Gerardo coefficients, but the calculated curve of $M_2(r=0, t)$ does not describe at all the experimental data and the calculated electron temperature $\langle T_e(t) \rangle$ is far from being constant at 293 °K, since it rises to 358 °K. At this pressure, for our experimental conditions, $M_1(t)$ and $n_e(t)$ are comparable. The values of α_2 and β can then be artificially increased; they compensate each other to reproduce $M_1(t)$ and $n_e(t)$, which is not true for $M_2(t)$. At higher gas pressure the disagreement between experimental and computed curves increases, but it is interesting to note that the Gerardo coefficients give, in general, a satisfactory agreement for $M_1(t, r=0)$ and for the early part of $\langle n_e^{\text{eff}}(t) \rangle$, which are precisely the two variables used by Johnson and Gerardo to determine their coefficients in the very early afterglow. Since they assume the electron-ion recombination coefficient α_2 does not depend on the electron density, they are obliged to take a very high pressure-dependent term and a very high constant term to describe the fast decay of the electron density in the early afterglow. These overestimated k_{02} and α_{c2} recombination coefficients make it impossible to reproduce the experimental $\langle n_e^{\text{eff}}(t) \rangle$ in the late afterglow especially when the pressure increases, even with a much too high β_{11} coefficient, calculated to compensate in the continuity equation of $M_1(t)$ the overestimated production of atomic metastables due to the recombination of He_2^+. It is not sufficient as a source term of electrons to compensate the overestimated recombination term in the continuity equation of $n_2(t)$. The overestimated values of β_{22}, β_{12}, and $D_{M_2} p_0$ correspond to very important destruction terms of $M_2(t)$ which are incompatible with the measured decay curves even with $\delta = 0.26$ Torr^{-2}/sec.

The set of coefficients obtained at 1.86 Torr by Pitchford *et al.*[84] has not been used, because the recombination rate coefficient α_2 is given in an empirical form, specific to this investigated pressure.

IX. DISCUSSION AND CONCLUSIONS

The method we have developed only applies when a large number of experimental data have been obtained at many pressures, exactly in the same discharge conditions for all the diagnostics used, and over a wide dynamic range for every variable. Further the method only applies if a mathematical model has been sufficiently elaborated to simulate with precision the evolution of all the characteristic measured physical quantities. Leffel, Hirsh, and Kerr[12] have proposed a complete analysis of the helium afterglow. They clearly presented the whole problem, identifying the important points: couplings, electron energy balance, role of the metastables, recombination mechanisms, spatial distributions, etc. This study led them to conclude that it was necessary to apply various diagnostics and to use a mathematical model including all the known elementary processes in a set of coupled partial differential equations.

Poukey, Gerardo, and Gusinow[86] have numeri-

cally solved a system of nine nonlinear coupled partial differential equations in order to show what are the main elementary processes that govern the helium afterglow at low gas pressure ($n_0 \sim 10^{16}$ cm^{-3}), high gas temperature (different from the ion temperature and from the electron temperature), and very high electron density ($n_e > 10^{14}$ cm^{-3}). For these experimental conditions they presented quantitatively the relative importance of the various reactions and processes. They showed that the atomic reactions and transport processes taken into account in the differential equations were realistic through a comparison of the computed curves with the experimental results obtained at the given pressure. The agreement they found is in fact quite good considering the large number of coefficients they imposed, many of which were poorly known in 1969. The method we have developed is comparable to that used by Poukey *et al.*: They imposed the value of the coefficients and concluded the predominance of a few mechanisms because of the satisfactory agreement between theory and experiment. On the contrary, we consider the main mechanisms in a helium afterglow are sufficiently well known for our experimental conditions to determine a system of differential equations able to simulate the evolution of the afterglow decay. The value of the unknown coefficients are deduced from the comparison of theory to experiment, when the calculated curves reproduce the measurements. The limited number of experimental data Poukey *et al.* could use at that time, at only one pressure, did not allow them to go as far as we did in the utilization of this method.

Collins[87] has been one of the first to calculate simultaneously a given number of rate coefficients related to the decay of the atomic and molecular metastables. He used a direct treatment of the experimental decay curves of the ion, metastable, and electron concentrations obtained at 3 Torr with Hurt.[41]

Collins measured, at different times in the afterglow and for each experimental curve, the first derivative and the absolute value of the variable considered. The system of coupled differential equations chosen to describe the afterglow was then replaced by a large number of systems of linear equations, leading to the unknown rate coefficients of the mechanisms are taken into account. Collins solved 135 systems of five linear equations with ten unknown variables, from which he determined eight coefficients. This method is very sensitive to the dispersion of the experimental points, depends very much on the absolute value of the measurements, and does not take into account the spatial distributions. At that time (1969) Collins neglected the influence of the electron temperature and did not have very accurate electron density measurements, but he was first to publish values of β_{22} and γ_2 deduced from experiment.

More recently Pitchford, Taylor, and Collins[84] applied the same method with a more accurate set of experimental results obtained at 1.86 Torr. At this pressure the molecular metastables do not play a dominant role and it is thus difficult to determine with good precision the rate coefficients of the processes which describe their evolution. The empirical form found for the part of the electron-ion recombination rate coefficient α_2 leading to the emission of molecular radiation from the lower states represents approximately 30% of the total recombination rate we measure in the electron density range 10^{12}–10^{10} cm^{-3}. The main disagreement is probably due to the molecular metastables: Collins *et al.* find molecular-metastable concentrations 2.4 times larger than ours for the same fractional absorption. At 1.86 Torr, they find exactly the same absolute densities for the atomic and molecular metastables, except in the very early afterglow (first 2 msec). Rates they report for the total collisional relaxation of molecular metastables are in good agreement with the values found in this work.

Johnson and Gerardo[29,30] have emphasized the production of electrons due to collisions between metastables. They have shown that if this source term is neglected in the interpretation of the electron concentration decay it leads to the underestimation of the recombination rate coefficient of the ion considered. But inversely, if all the destruction terms for metastables are neglected except collisions between metastables, as Johnson and Gerardo did, the corresponding β coefficients are overestimated and subsequently the recombination rate coefficient is also overestimated. Johnson and Gerardo determined the electron-ion recombination rate coefficient of He_2^+, in the pressure range 15–55 Torr, in a 12.8-cm-i.d. cylindrical cell, using the electron-heating-pulse technique. The electrons were heated with a current pulse of 0.1 to 1.0 A and 200-μsec duration, during the first 800 μsec in the afterglow.

The over-all interpretation of their measurements lies on the assumption that the electron-ion recombination rate coefficient of He_2^+ is not electron density dependent. Three arguments are advanced to justify this assumption:

(a) The apparent recombination rate (α_{eff}) is constant with time. As a matter of fact the plot of $[n_e(t)]^{-1}$ at 15, 30, and 45 Torr gives a straight line over the first 5 msec, but our interpretation is different. Johnson and Gerardo neglect the

influence of the electron temperature, which is probably quite high for their experimental conditions. The free diffusion of hot electrons is negligible and the atomic-metastable concentrations are high, being for instance twice the electron concentration at 25 Torr even though the molecular metastables are neglected. For the same metastable-to-electron concentration ratio the electron temperature must be higher in their experiment than in ours and must relax much more slowly, particularly if the average gas temperature is raised by 15 °C. This elevated electron temperature decreases considerably the importance of the term $k_{e2}n_e(r,t)[T_e(r,t)/293]^{-9/2}$, which becomes negligible with regard to the neutral-assisted recombination term, during the first five msec. The influence of the electron temperature explains the linear variation of $[n_e(t)]^{-1}$ as a function of time, except during the first 300 μsec, where the electron temperature is so high that the recombination is completely inhibited.

(b) The second argument is that the measured value of α_2 does not vary with electron density. The recombination rate is determined in the very early afterglow between 200 and 800 μsec; the electron density range covered during that time is at the maximum a factor of 2.

(c) Finally they argue that the measured intensity of the $3p\,^3\pi_g \rightarrow 2s\,^3\Sigma_u^+$, 4650-Å band is always proportional to the square of the electron density, when a purely collisional-radiative electron-stabilized recombination model leads to an electron density dependence higher than 2, becoming proportional to n_e^3 at high electron density. Actually when the inelastic collisions between neutral particles are included in the collisional-radiative model[60,61] the electron concentration dependences of the population densities of the excited states decrease and tend to 2 even for the lowest excited levels, when the pressure is high enough. This influence of the inelastic collisions with a ground-state atom is even stronger if the vibrational and rotational energy levels are included in the collisional-radiative recombination model. Finally the influence of the electron temperature also tends to decrease the electron density dependence of the population concentrations of the excited states and can even lead to dependences smaller than 2. The proportionality to the square of the electron density of the measured emitted band (4650 Å) does not prove that α_2 does not depend on n_e.

The other basic assumption of Johnson and Gerardo in the interpretation of their measurements is that the source term S of electrons is not modified during the heating pulse, the temperature of which is about 1500 °K. A detailed study of what happens during such a heating pulse applied to the helium afterglow has never been performed, because of the complexity of the problem. Our computer program is now able to simulate such an event and results will be discussed in a future publication. It is an "*a priori* assumption" to propose that only the kinetic energy of the background electron gas is slightly increased without any other change during the heating pulse.

In these first two papers[29,30] Johnson and Gerardo determine a very strong value of the recombination rate coefficient α_2, giving a considerable importance to collisions between metastables. However, they have neglected the electron temperature increase due to this enormous source term of very energetic electrons and attributed a dominant role to the atomic and molecular metastables which were not measured. They obtained

$$(\alpha_2)_{JG} = 1.1\times10^{-8} + 1.25\times10^{-26}n_0 .$$

In two other papers[46,88] Johnson and Gerardo determined the rate coefficient of collisions between two metastables. They started with the overestimated value of α_2, identified as "dissociative recombination," and still neglected the influence of the electron temperature although it was evaluated to be 450 °K. They considered the atomic and molecular metastables to be indistinguishable ($\beta = \beta_{11} = \beta_{12} = \beta_{22}$), only measured the decay of the triplet atomic metastables, and neglected all the metastable destruction terms except ionizing mutual collisions. In addition they assumed that $M_1(t)$, $M_2(t)$, and $n_e(t)$ decay identically as a function of time, a relationship which is not supported by experimental evidence.

A first value of β is given by the solution of

$$\frac{\partial n_e}{\partial t} = -\alpha n_e^2 + \tfrac{1}{2}\beta M^2 = -\alpha_{\rm eff} n_e^2 ,$$

where α and $\alpha_{\rm eff}$ are the values previously published.[29,30]. A second value of β is determined by solving

$$\frac{\partial M}{\partial t} = -\beta M^2 + k\alpha n_e^2 = -\beta_{\rm eff} M^2 ,$$

where k was arbitrarily set to 1 to represent the total fraction of recombination events which result in metastable species, α has the above value and $\beta_{\rm eff}$ is deduced from $M^{-1}(t)$. They consider that this second determination is independent of the first one. They find in both cases $\beta = (4.5 \pm 1.0)\times10^{-9}$ cm^3/sec. This rate coefficient actually does not correspond to any given mechanism but rather is a consequence of the overestimation of the recombination rate coefficient α_2.

Boulmer *et al.*[31] have applied the same experimental technique at pressures from 20 to 30 Torr. Their conclusions are in disagreement with the

results of Johnson and Gerardo (see Table I) for α_2: The recombination rate coefficient α_2 is not pressure dependent, but depends on electron density. The same experimental technique leads to completely different results when the number of mechanisms taken into account in the interpretation of the helium afterglow is too limited and when the number of experimental data is too small. This is one of the consequences of the strong couplings occurring in this ionized gas.

The main goal of this work was to determine both the absolute value and the dependences of the electron-ion recombination rate coefficient of He_2^+ taking into account all the mechanisms which govern the evolution of the helium afterglow. One of the most important results is the confirmation of the dominant role played by the inelastic collisions including a ground-state atom [(13) and (18)–(20)] in the recombination of He_2^+, which we had shown for the first time in 1970.[25] We also confirm the electron density dependence of α_2, the corresponding recombination rate being even twice as big as the value we published in 1970 when the influence of the metastables was neglected. The electron temperature dependences found for α_2 show, in addition to the above results, that the recombination of molecular ions He_2^+ and electrons is *collisional-radiative*.

We also confirm that a large proportion (70%) of the recombined He_2^+ ions leads to the production of atomic triplet metastables, as had been first published by Lambert and Cheret.[85] We show that 20%, at 5 Torr, of these recombined He_2^+ ions give molecular metastables and that this percentage decreases when the pressure is increased and tends to zero above 40 Torr, the unique source of molecular metastables being then the atomic-metastable conversion (24).

The characteristics of the theoretical electron-He_2^+ recombination model will be quite well defined if we give in addition to the above results the following features: (i) The measured rotational temperatures are always abnormally high with respect to the gas temperature and decay very slowly; (ii) all the observed molecular bands (up to principal quantum number $p = 20$) decay identically with time; (iii) for pressures above 5 Torr the population densities of the excited electronic states of the molecule are proportional to the square of the electron density even for the lowest quantum levels, except when the electron temperature is higher than T_g. The theoretical model of the recombination of molecular ions He_2^+ and electrons is of the collisional-radiative type with a strong influence of inelastic collisions with ground-state atoms [(13) and (18)–(20)], inelastic collisions with electrons [(12) and (17)], and radiative processes [(16) and (11)]. Although the molecular ions are always produced in highly excited vibrational states the dissociative recombination (22) is extremely small, if not negligible, the measured value of the constant term of α_2 being always very small. Vibrational relaxation of molecular ions in collisions with ground-state atoms or through processes (15) would have to be taken into account in the theoretical model.

In order to explain that 70% of recombined molecular ions produce atomic triplet metastables it would be necessary to include a dissociative potential-energy curve among the lowest electronic states of the molecule (principle quantum number 4 or 5) leading, for instance, to the atomic energy level $2\,^3P$. This could also explain the identical decay of the 10 831.6-Å atomic line with the molecular bands, as has been observed by Collins.[89]

Finally, this theoretical model should be able to give an interpretation of the increasing percentage with pressure of recombined molecular ions (10% at 5 Torr, and 30% at 40 Torr and above) which do not produce any metastable state: The influence of the stabilization through the singlet molecular system, leading to the dissociative ground state in radiative deexcitation, probably increases with pressure.

The transitions induced in collisions with ground-state atoms are very important and are able to explain all the following optical observations: (i) identical decay of all the molecular bands, (ii) proportionality of the population densities of the excited molecular states to the square of the electron concentration, and (iii) population density distributions of the rotational levels out of equilibrium. They imply taking into account simultaneously all the transitions between electronic, vibrational, and rotational states of the molecule. Independent of the size of the computer program, the main difficulties in building such a theoretical model would be to determine the potential-energy curves of the excited states and to calculate the unknown cross sections of the important processes such as (13) and (18)–(20), along with the ionization probabilities of the autoionizing levels. This model has no relation with the direct or indirect dissociative recombination as was defined, for example, by Biondi.[90] This study of the electron-ion recombination rate coefficient of He_2^+ led us to analyze the over-all helium afterglow and to understand all the correlations occurring between the different mechanisms which govern the relaxation of this ionized gas. It has been compulsory to develop various diagnostics in order to measure all the significant parameters and to elaborate a mathematical model to reproduce

all the experimental data in order to simulate the evolution with time of the afterglow.

The detailed study of the various particle concentrations and electron energy balance as a function of time and space, included in the method we have developed, has shown it is now possible in an ionized gas to determine rate coefficients and new mechanisms which cannot be presently obtained for other experimental conditions. It is also possible to give, at every pressure, the relative importance as a function of time in the afterglow of the various mechanisms and transport processes. This work has indicated the influence of the spatial distributions and especially of the electron temperature profiles. The role of the non-Maxwellian electrons has been shown in the radiometric measurements and calculated by the computer program. Measurements of the electron energy distribution functions as a function of time and space are in progress.

Finally this study has proved that the determination of one elementary process or a single rate coefficient during the relaxation of an ionized gas, where couplings are so strong, obliges one to know all the significant mechanisms and to measure their rate coefficients simultaneously. The exact simulation of the helium afterglow corresponding to an excellent fit between the computed curves and more than 40 000 experimental data points, covering a large range of variation of experimental conditions, indicates strongly that the mechanisms taken into account correctly describe this medium, further justifies the assumption that the heavy molecular ions do not play a significant role at room temperature, and finally proves that the rate coefficients integrated on the electron energy distribution functions are well determined. The rate coefficients obtained in this work are in good agreement with available theoretical values. This method can be applied to a different gas and extended in helium to many other experimental conditions.

ACKNOWLEDGMENTS

The authors wish to express their deepest appreciation to Dr. Jacques Berlande for his constant advice and encouragement during the course of this work. They would like to acknowledge Dr. W. E. Wells, Dr. H. Helm, and Dr. M. Jardino for their very efficient contributions to this work during their stay in Saclay. They wish to express their gratitude to H. Jeudon and her group and more especially to J. P. Felix and M. Ahrweiller for important contributions in the accomplishment of the electronics of this experiment. It is a pleasure to thank R. Durand for his aid in building the apparatus and obtaining data. The skill of the glass-blower J. Delcher made possible the excellent performance of the vacuum system. The authors are also grateful to Dr. A. B. Forge and Dr. J. Lieutaud of the C.I.S.I. in Saclay for their help in computer programming. They are greatly indebted to Dr. C. Manus for numerous useful discussions and helpful comments. They gratefully acknowledge Professor Donald E. Kerr for his many suggestions about the optical measurements during his visit in their laboratory.

APPENDIX

The electron-ion collision frequency $\nu_{ei}(v)$ is

$$\nu_{ei}(v) = \frac{4\pi e^4}{m^2 \bar{v}_i^2} n_i(r,t) \frac{1}{v} R\left(\frac{v}{\bar{v}_i}\right) \times \ln\left[\frac{mk^{1/2}}{2e^3\pi^{1/2}}\left(\frac{T_e(r,t)}{n_e(r,t)}\right)^{1/2} v^2\right],$$

with

$$\bar{v}_i = \left(\frac{2k}{M} T_g\right)^{1/2}$$

and

$$R\left(\frac{v}{\bar{v}_i}\right) = \frac{4}{\pi^{1/2}} \frac{\bar{v}_i^2}{v^2} \int_0^{v/\bar{v}_i} e^{-x^2} x^2 \, dx,$$

where $n_i(r,t)$ is the ion concentration of mass M. In first approximation the elastic electron-ion collision frequency can be simplified if $\frac{1}{2}mv^2$ is replaced by $kT_e(r,t)$ in the expression of the logarithm and if we assume $v/\bar{v}_i \gg 1$, as is always verified in our experimental conditions. In that case

$$\nu_{ei}^a(v) = \frac{4\pi e^4}{m^2} n_i(r,t) \frac{1}{v^3} \ln\left(\frac{k^{3/2}}{e^3\pi^{1/2}} \frac{[T_e(r,t)]^{3/2}}{[n_e(r,t)]^{1/2}}\right).$$

The average approximated elastic electron-ion collision frequency integrated on the Maxwellian distribution function $f_0(v)$ is written as

$$\langle \nu_{ei}^a(r,t) \rangle = \frac{16\pi^2 e^4}{3kmT_e(r,t) n_e(r,t)} [n_1(r,t) + \tfrac{1}{2} n_2(r,t)] \times \ln\Lambda(r,t) \int_0^\infty v f_0(v) \, dv,$$

with

$$\Lambda(r,t) = \frac{k^{3/2}}{e^3\pi^{1/2}} \frac{[T_e(r,t)]^{3/2}}{[n_e(r,t)]^{1/2}}$$

and

$$\int_0^\infty 4\pi v^2 f_0(v) \, dv = n_e(r,t),$$

which is a very good approximation under our experimental conditions, better than 10^{-3}.

$$\langle \nu_{ei}^{a}(r,t)\rangle = \frac{8e^4}{3k}\left(\frac{\pi}{2km}\right)^{1/2}[n_1(r,t)+\tfrac{1}{2}n_2(r,t)]\,\frac{1}{[T_e(r,t)]^{3/2}}\ln\Lambda(r,t),$$

$$\left(\frac{\partial T_e(r,t)}{\partial t}\right)_{ei} = -b_2[n_1(r,t)+\tfrac{1}{2}n_2(r,t)]\,\frac{T_e(r,t)-T_g}{[T_e(r,t)]^{3/2}}\,\ln\left(b_3\frac{[T_e(r,t)]^{3/2}}{[n_e(r,t)]^{1/2}}\right),$$

with

$$b_2 = \frac{16e^4}{3kM}\left(\frac{\pi m}{2k}\right)^{1/2} = 9.89\times10^{-4}\ \text{cgs},$$

$$b_3 = k^{3/2}/e^3\pi^{1/2} = 8.26\times10^{3}\ \text{cgs}.$$

[1]M. A. Biondi, Rev. Sci. Instrum. 22, 500 (1951).
[2]M. A. Biondi and S. C. Brown, Phys. Rev. 75, 1700 (1949).
[3]A. V. Phelps and S. C. Brown, Phys. Rev. 86, 102 (1952).
[4]J. A. Hornbeck and J. P. Molnar, Phys. Rev. 84, 621 (1951).
[5]D. Smith and M. J. Copsey, J. Phys. B 1, 650 (1968).
[6]M. A. Biondi, Phys. Rev. 82, 453 (1951).
[7]A. V. Phelps, Phys. Rev. 99, 1307 (1955).
[8]E. P. Gray and D. E. Kerr, Bull. Am. Phys. Soc. 5, 372 (1960).
[9]D. R. Bates and A. E. Kingston, Proc. R. Soc. Lond. 279, 10 (1964).
[10]D. R. Bates, A. E. Kingston, and R. W. P. McWhirter, Proc. R. Soc. A 267, 297 (1962).
[11]J. C. Ingraham and S. C. Brown, Phys. Rev. 138, 1015 (1965).
[12]C. S. Leffel, M. N. Hirsh, and D. E. Kerr, report of The Johns Hopkins University, Baltimore, Maryland (unpublished).
[13]E. Hinnov and J. G. Hirschberg, Phys. Rev. 125, 795 (1962).
[14]R. A. Gerber, G. F. Sauter, and H. J. Oskam, Physica 32, 217 (1966).
[15]C. B. Collins and W. B. Hurt, Phys. Rev. 167, 166 (1968).
[16]C. B. Collins, H. S. Hicks, W. E. Wells, and R. Burton, Phys. Rev. A 6, 1545 (1972).
[17]D. E. Kerr and C. S. Leffel, Bull. Am. Phys. Soc. 7, 131 (1962).
[18]H. J. Oskam and V. R. Mittelstadt, Phys. Rev. 132, 1445 (1963).
[19]W. A. Rogers and M. A. Biondi, Phys. Rev. 134, 1215 (1964).
[20]C. B. Collins and W. W. Robertson, J. Chem. Phys. 40, 2202 (1964).
[21]R. S. Mulliken, Phys. Rev. 136, 962 (1964).
[22]E. E. Ferguson, F. C. Fehsenfeld, and A. L. Schmeltekopf, Phys. Rev. 138, 381 (1965).
[23]C. L. Chen, C. C. Leiby, and L. Goldstein, Phys. Rev. 121, 1391 (1961).
[24]R. Deloche, A. Gonfalone, and M. Cheret, C. R. Acad. Sci. (Paris) 267, 934 (1968).
[25]J. Berlande, M. Cheret, R. Deloche, A. Gonfalone, and C. Manus, Phys. Rev. A 1, 887 (1970).
[26]J. Stevefelt, Proceedings of the Fourteenth International Conference on Phenomina in Ionized Gases, Bucharest, 1969 (unpublished).
[27]R. A. Johnson, B. T. McClure and R. B. Holt, Phys. Rev. 80, 376 (1950).
[28]C. B. Collins, H. S. Hicks, and W. E. Wells, Phys. Rev. A 2, 797 (1970).
[29]A. W. Johnson and J. B. Gerardo, Phys. Rev. Lett. 27, 835 (1971).
[30]A. W. Johnson and J. B. Gerardo, Phys. Rev. A 5, 1410 (1972).
[31]J. Boulmer, P. Davy, J. F. Delpech, and J. C. Gauthier, Phys. Rev. Lett. 30, 199 (1973).
[32]M. A. Gusinow, R. A. Gerber, and J. B. Gerardo, Phys. Rev. Lett. 25, 1248 (1970).
[33]H. F. Wellenstein, and W. W. Robertson, J. Chem. Phys. 56, 1077 (1972).
[34]C. B. Collins, B. W. Johnson, and M. J. Shaw, J. Chem. Phys. 57, 5310 (1972).
[35]J. Stevefelt, Phys. Rev. A 8, 2507 (1973).
[36]R. Brout, J. Chem. Phys. 22, 934 (1954).
[37]C. B. Collins, report of the University of Texas at Dallas, 1971 (unpublished).
[38]A. V. Phelps and J. P. Molnar, Phys. Rev. 89, 1203 (1953).
[39]H. Myers, Phys. Rev. 130, 1639 (1963).
[40]P. L. Pakhomov, G. P. Reznikov, and I. Ya. Fugol, Opt. Spectrosk. 20, 10 (1966) [Opt. Spectrosc. 20, 5 (1966)].
[41]C. B. Collins and W. B. Hurt, Phys. Rev. 177, 257 (1969).
[42]W. B. Hurt, J. Chem. Phys. 45, 2713 (1966).
[43]E. R. Mosburg, Phys. Rev. 152, 166 (1966).
[44]P. A. Miller, J. T. Verdeyen, and B. E. Cherrington, Phys. Rev. A 4, 692 (1971).
[45]W. B. Peatman and J. P. Barach, J. Chem. Phys. 58, 2638 (1973).
[46]A. W. Johnson and J. B. Gerardo, Phys. Rev. A 7, 925 (1973).
[47]B. J. Garrison, W. H. Miller, and H. F. Schaefer, J. Chem. Phys. 59, 3193 (1973).
[48]D. R. Bates, K. L. Bell, and A. E. Kingston, Proc. Phys. Soc. Lond. 91, 288 (1967).
[49]G. J. Schultz and R. E. Fox, Phys. Rev. 106, 1179 (1957).
[50]D. J. T. Morrison and M. R. H. Rudge, Proc. Phys. Soc. Lond. 91, 565 (1967).
[51]P. Monchicourt, thesis (University Paris VII, 1972) (unpublished).
[52]M. Gryzinski, Phys. Rev. 115, 374 (1959).
[53]R. K. Nesbet, R. S. Oberoi, and J. N. Bardsley, Chem.

Phys. Lett. 25, 587 (1974).
[54]R. S. Oberoi and R. K. Nesbet, Phys. Rev. A 8, 2969 (1973).
[55]H. H. Brongersma, F. W. E. Knoop, and C. Backs, Chem. Phys. Lett. 13, 16 (1972).
[56]W. E. Wells, P. Monchicourt, R. Deloche, and J. Berlande, Phys. Rev. A 8, 381 (1973).
[57]F. R. Castell and M. A. Biondi, paper in LA 7, G. E. C., 1974 (unpublished).
[58]P. Monchicourt, M. Touzeau, and W. E. Wells, J. Phys. (Paris) 34, 145 (1973).
[59]A. B. Blagoev, Yu. M. Kagan, N. B. Kolokolov, and R. I. Lyagushenko, Zh. Tekh. Fiz. 44, 333 (1974) [Sov. Phys.-Tech. Phys. 19, 211 (1974)].
[60]R. Deloche, C. R. Acad. Sci. (Paris) 266, 664 (1968).
[61]C. B. Collins, Phys. Rev. 177, 254 (1969).
[62]J. P. Shkarofsky, Can. J. Phys. 39, 1619 (1961).
[63]J. C. Gauthier, thèse 3è cycle (Orsay, 1970) (unpublished).
[64]M. Ahrweiller, Nucl. Instrum. Methods 96, 205 (1971).
[65]J. M. Anderson and L. Goldstein, Phys. Rev. 100, 1037 (1955).
[66]R. Deloche, W. E. Wells, P. Monchicourt, and J. Berlande, J. Phys. B 6, 1881 (1973).
[67]G. Bekefi, *Radiation Processes in Plasmas* (Wiley, New York, 1966).
[68]F. Lambert, Ph.D. (University Paris VI, 1975) (unpublished).
[69]M. Jardino, thesis (University Paris-Sud, 1974) (unpublished).
[70]B. L. Wright and G. Bekefi, Phys. Fluids 14, 1764 (1971).
[71]A. C. G. Mitchell and M. W. Zemansky, *Resonance Radiation and Exchange Atoms* (Cambridge U. P., Cambridge, England, 1961).
[72]F. Lambert, C. R. Acad. Sci. (Paris) 274, 1406 (1972).
[73]J. Brochard, R. Chabbal, H. Chantrel, and P. Jacquinot, J. Phys. Radium 18, 596 (1957).
[74]W. C. Martin, J. Res. Natl. Bur. Stand. (U.S.) 64, 9 (1960).
[75]U. Pittack, Z. Astrophys. 190 (1964).
[76]H. G. Kuhn and J. M. Vaughan, Proc. R. Soc. Lond. 277, 297 (1963).
[77]J. M. Vaughan, Proc. R. Soc. Lond. 295, 164 (1966).
[78]J. Stevefelt and F. Robben, Phys. Rev. A 5, 1502 (1972).
[79]D. R. Bates and A. Damgaard, Philos. Trans. R. Soc. Lond. A 242, 101 (1949).
[80]A. B. Callear and R. E. M. Hedges, Trans. Faraday Soc. 66, 2921 (1970).
[81]R. W. Huggins and J. H. Cahn, J. Appl. Phys. 38, 180 (1967).
[82]M. Jardino, F. Lambert, and R. Deloche, C. R. Acad. Sci. (Paris) 278, 1087 (1974).
[83]M. A. Gusinow and R. A. Gerber, Phys. Rev. A 2, 1973 (1970).
[84]L. C. Pitchford, K. N. Taylor, and C. B. Collins, J. Phys. B 8, 142 (1975).
[85]M. Cheret and F. Lambert, C. R. Acad. Sci. (Paris) 275, 77 (1972).
[86]J. W. Poukey, J. B. Gerardo, and M. A. Gusinow, Phys. Rev. 179, 211 (1969).
[87]C. B. Collins, in *Proceedings of the Eighth International Conference on Phenomina in Ionized Gases, Vienna, 1967* (Springer, Berlin, 1967), contributed paper 1.2.4.
[88]A. W. Johnson and J. B. Gerardo, Phys. Rev. Lett. 28, 1096 (1972).
[89]C. B. Collins and W. B. Hurt, Phys. Rev. 179, 203 (1969).
[90]M. A. Biondi, SRCC report No. 192, University of Pittsburgh, 1973 (unpublished).
[91]I. Ya. Fugol, O. N. Grigorashchenko, and D. A. Myshkis, Zh. Eksp. Teor. Fiz. 60, 423 (1971) [Sov. Phys.-JETP 33, 227 (1971)].